Rijks*universiteit* **Faculteit der Wiskunde en Natuurwetenschappen** *16th January 2012*
Groningen **Technische Natuurkunde**

Spin Dephasing Anisotropy in Bulk Gallium Arsenide

RuG

Master thesis by: **Olger Victor Zwier**

Research Group: Physics of Nanodevices,

Subgroup Leader: prof.dr.ir. C.H. van der Wal

Supervisor: drs. S. Denega

Referent: dr. T. Banerjee

Period: June 2010 - June 2011

Spin Dephasing Anisotropy in bulk and two-dimensional GaAs

Olger Victor Zwier

16th January 2012

Abstract

In the first part of this thesis, the origins of Spin Dephasing Anisotropy (SDA) in semiconductors are discussed, to pave the way for a design and realization of a device, meant to characterize SDA in two-dimensional and bulk electron gasses in GaAs. The anisotropy will be investigated in quasi-ballistic channels, oriented in four different crystallographic directions. Due to the nature of the Spin-Orbit fields (SO-fields) in the material, a strong dependency of SDA on channel orientation is expected. Passing currents through these channels, applying external magnetic fields, and top gating are all possible in situ, to analyze their expected effects on the SDA. The fabrication was not fully completed at the time of writing, but the most crucial step of wet etching micrometer-sized structures had been fully characterized and perfected, and the remaining steps had been tested for, leaving very little work yet to be completed.

To support these and previous measurements on bulk electron gas measurements, the second part of this thesis presents a numerical study of the electron spin dephasing time T_2^* in quasi-ballistic wires of bulk GaAs material. The study assumes that dephasing occurs due to spin-orbit fields from a bulk Dresselhaus term and a Rashba term in wires with either specular or non-specular momentum scattering on the walls of the wire. With a similar magnitude for the Dresselhaus and Rashba effect our results show the longest T_2^* values for wires in [110] direction. This is consistent with the dependence of T_2^* on the crystal orientation of wires that was observed in recent experiments. However, a comparison with results for random momentum scattering on the wire edges reveals that the mechanism behind the spin dephasing anisotropy differs from the analogues effect in wires with two-dimensional electron systems: instead of a confinement-induced motional-narrowing effect, spin dephasing anisotropy now results from the interplay between repetitive electron trajectories in the wire and the anisotropy in the spin orbit fields. This points to a mechanism that has similarities with the phenomenon of ballistic spin resonance that can occur in wires based on 2D electron systems. A large part of the simulations also concerned studying the magnetic field dependence of this phenomenon with simulations that account for the field-induced cyclotron motion of electrons.

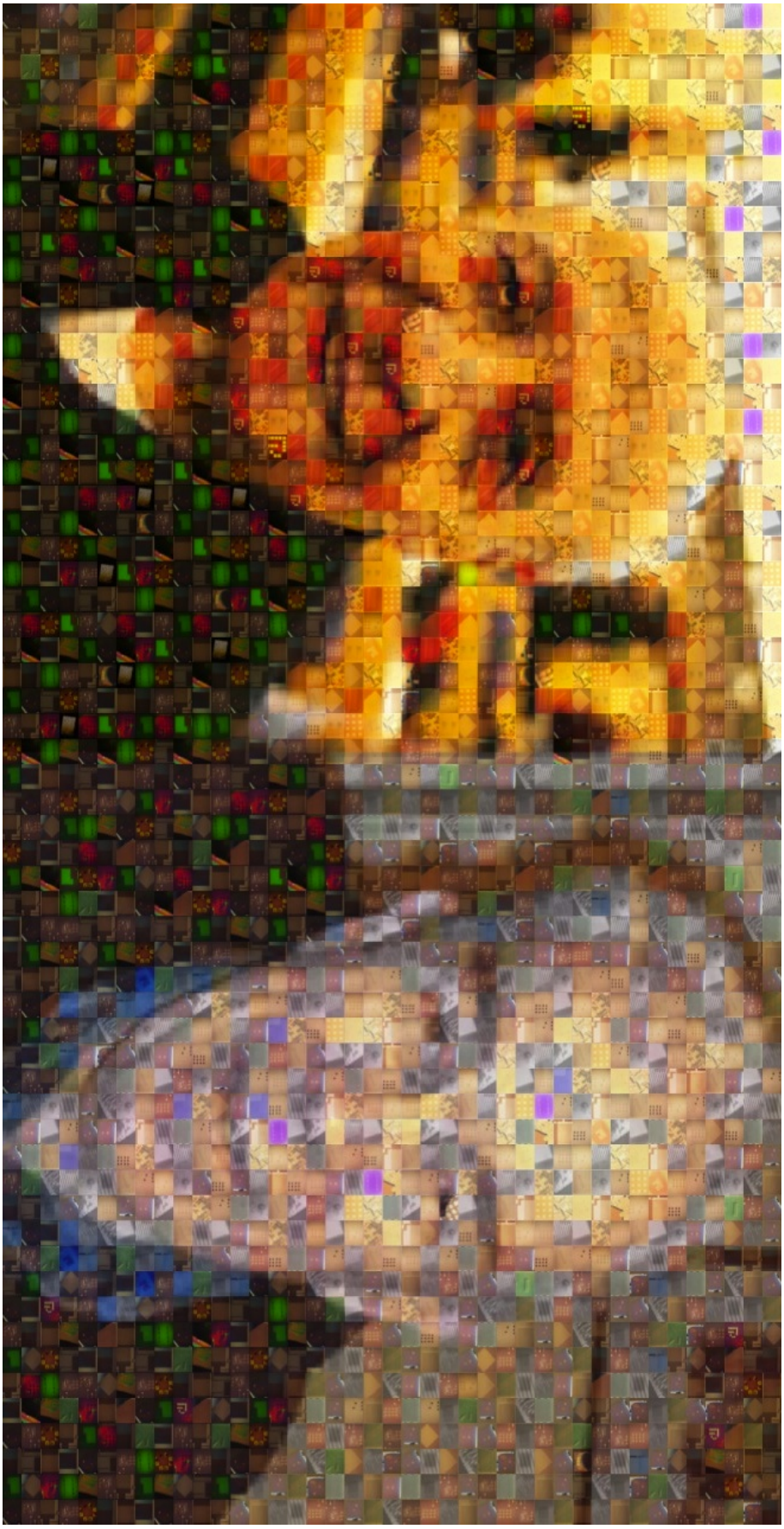

Figure 1: Top: E.I. Rashba, namesake of the Rashba SO-term. Bottom: G. Dresselhaus, namesake of the Dresselhaus SO-term. Mosaic created using optical microscope and SEM images, made during this master project.

Contents

Chapter 1

Introduction

If a human being is a particle's way of thinking about particles, one could say they have come a long way in figuring themselves out. The property of "spin", which began to be discovered in the 1920's, is one of their triumphs of self-awareness. A quintessential quantum property obeying many of the same rules as angular momentum, the spin is an extra degree of freedom of an elementary particle, and has no easily understood classical, everyday explanation. Yet, very importantly for all that will follow here, a particle's spin is directly associated with a particle's magnetic moment, and will therefore have interplay with any magnetic fields the particle may encounter.

This work will be concerned with the spins of electrons, and the reason for studying the physics of these lies in their potential use as information carriers. Electron spin ensembles, having some initial collective alignment, will lose this alignment because of a multitude of individual interactions, causing their average spin to decay in time. This is termed spin dephasing. Thus, to be able to utilize ensembles of spins as signals in a device, it is necessary to accomplish several things. Firstly, the spins need to be aligned, for example by passing electrons through a ferromagnet (in which all spins have a net alignment), or by optically exciting them with polarized light (which transfers the photon polarization into spin orientation). Next, this alignment needs to be maintained for as long as possible, meaning any mechanisms that disalign the spins must be countered or suppressed. Lastly, the spin signal needs to be read out again, for example using non-local voltage measurement techniques (measuring a diffused spin population through ferromagnets), or by optical reflection measurements (which observe the spin population-dependent rotation of linearly polarized light).

Furthermore, the interactions that reduce the spin alignment are highly dependent on the material the electrons are located in. The material used throughout this work is crystalline gallium arsenide (GaAs), a III-V semiconductor with the zinc-blende structure, grown epitaxially to have both 3D and 2D electron gas populations. In such populations in GaAs, there is inherent anisotropy in the fields the moving particles experience, which carries over to anisotropy in dephasing rates, depending on how these ensembles are exactly spatially confined. The goal of this research is to characterize this spin dephasing anisotropy (SDA), for free electrons confined to narrow wires, oriented in different directions, both in 2D and in bulk populations. Especially for the bulk electrons, little is already known. Also the influence of flowing currents, gating, doping and static external magnetic fields were investigated. The approach is twofold: we set out to do both real optical experiments on self-fabricated devices, and perform extensive numerical experiments.

In Chapter 2, the theory of SDA in GaAs is explained, as are the different techniques to manipulate this SDA. Having made explicit the general concepts, this thesis will then split into two distinct halves. Chapter 3 will discuss the principles and fabrication of a device with which to measure spin ensemble evolution in time. Chapter 4 will present results of extensive simulations performed in Matlab on ensembles of electrons in bulk GaAs.

This work was performed as a Master Research in the Physics of Nanodevices group at the Rijksuniversiteit Groningen, under the supervision of Sergii Denega and Caspar van der Wal.

Chapter 2

Spin dephasing anisotropy in bulk crystalline GaAs

2.1 Introduction

In this chapter, the theory and methods that form the basis of our research are discussed. Section 2.2 will discuss the basics of the interactions between electron motions and their spins in GaAs. Section 2.3 will list and dicuss the different methods we have of influencing these interactions. Then, Section 2.4 will briefly illustrate the type of measurement used to extract information on the electron populations' spins.

2.2 Spin-orbit interaction in GaAs

In the case of spin signals in semiconductors, we look at ensembles of electrons excited to or above the conduction band (so-called "free" electrons). These might be excited there (e.g. optically or thermally), or reside there naturally (e.g. in a 2-dimensional electron gas). The dominant mechanism causing such ensembles' spins to dephase is termed spin-orbit interaction (SOI). This SOI can be any coupling of a particle's spin to its motion. In GaAs, this coupling comes from static electric fields being present in the material, due to asymmetries in the crystal structure [1]. The reason the spins, being *magnetic* moments, couple to these electric field is due to their moving at significant fractions of the speed of light (the "orbit"), leading to an apparent magnetic field in the electron frame of reference (through relativistic correction). The electron spin also exists in the electron frame of reference (divided by a factor 2, the Thomas factor), and it will precess around the magnetic field it sees there, with angular frequency $\omega = \frac{B_{SO}q}{m}$ (the "coupling", where B_{SO} is the apparent magnetic field, q is electron charge, and m is electron mass).

In GaAs, the total SO-field is made up of two contributions, anisotropic in particle motion direction. A note ahead: for these directions, throughout this thesis standard Miller index notation will be employed, with [100] representing the x-direction, [010] the y-direction, and [001] the z-direction in the GaAs zinc-blende crystal structure.

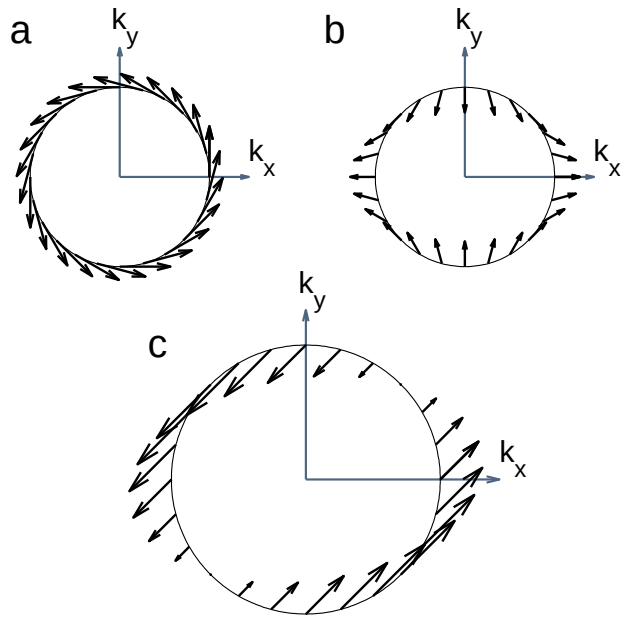

Figure 2.1: a) Plot of the Rashba spin-orbit field in Fermi space on the Fermi k-vector, with the circular symmetry clearly visible. b) Plot as in Figure 2.1(a), but for the linear Dresselhaus field. c) Plot of the sum of the Rashba and linear Dresselhaus fields, with their prefactors being equal. The fields can be seen to add up in the $[\bar{1}10]$ direction, and cancel in the [110] direction.

The first contribution, stemming from structural inversion asymmetry in the growth direction of an epitaxially grown wafer of GaAs, is termed the Rashba field [2]:

$$\vec{B}_R = C_R(\hat{x}k_y - \hat{y}k_x). \tag{2.1}$$

Here C_R is the prefactor determining the magnitude of the effect, k_x and k_y are the particle's wavevector, in the $\hat{x}$- and $\hat{y}$-directions, respectively. The second field, stemming from inversion assymetry in the bulk crystal structure, is termed the cubic Dresselhaus field [3, 2] (with "cubic" referring to the triple products of the wavevectors seen in the following equation):

$$\vec{B}_{D3} = C_{D3}(\hat{x}k_x(k_y^2 - k_z^2) + \hat{y}k_y(k_z^2 - k_x^2) + \hat{z}k_z(k_x^2 - k_y^2)). \tag{2.2}$$

Here C_{D3} is the cubic Dresselhaus prefactor. These are the two SO-field terms present in general, bulk GaAs. One can now confine the electrons in one dimension (in our case, orthogonal to the sample growth direction $\hat{z}$), meaning the electrons are quantized in this third direction, and can not classically move there. This is the definition of a *2 dimensional electron gas* (2DEG). It entails that k_z becomes very large (since it's inversely proportional to the confinement width), and so $k_z^2 >> k_x^2 + k_y^2$, and k_z^2 can be taken to be so large to be approximately constant. From the cubic Dresselhaus field we then derive a *linear* Dresselhaus field:

$$\vec{B}_{D1} = C_{D1}(-\hat{x}k_x + \hat{y}k_y). \tag{2.3}$$

The Rashba and linear Dresselhaus terms are displayed in Figures 2.1(a) and 2.1(b), respectively, where the SO-fields are plotted on the Fermi circle in 2-dimensional k-space. From Figure 2.1(c), showing the total SO-field with prefactors C_R and C_{D1} being exactly equal (a viable possibility in GaAs quantum wells), it can be seen that the two are opposed in the [110] direction, and add up in the $[\bar{1}10]$ direction. An electron propagating in the [110] direction would therefore precess much slower than one moving in another direction, and so an ensemble of electrons moving *predominantly* in this direction would be expected to dephase slower than an ensemble moving predominantly anywhere else. This anisotropy is what we wish to probe, and manipulate. It has been central in many theoretical proposals [4, 5, 6, 7, 8, 9] aimed at suppressing spin dephasing. Such a suppression has been observed with quasi-1D wire systems based on 2-dimensional GaAs materials [10, 11, 12], where the spin dephasing time showed a dependence on the crystal orientation in the wires.

One of these experiments also showed the unexpected result that the spin dephasing time T_2^* for electrons in wires etched out of *bulk* GaAs (electron channels of 1μm wide and many hundreds of micrometers long, with these boundaries etched into a 1μm deep layer containing free electrons) also has a dependence on the crystal orientation in the wires [12]. Also here, the longest T_2^* values were observed for wires along the [110] direction. Initial numerical studies of this effect that were reported in the original publication on the experiment indicated that the spin dephasing anisotropy (SDA) in these wires also relies on a cancelation between two spin-orbit terms. In this case, these are the cubic Dresselhaus [3] term and the Rashba term [2]. While the Rashba term has mostly been described in the context of 2D confined electron systems, for micron-thick bulk layers it can also play a role, when energy band bending is present in the material. In the reported experiment there was an unidirectional electric field present in a micron-thick bulk layer near the wafer surface, providing the required bending.

2.3 Manipulating the Spin Dephasing Anisotropy

For manipulation of the SDA, there are several ways in which to tune the relative strengths of the Rashba and Dresselhaus SO-fields: electron confinement, passing a current through the electron spin population, gating of the sample, altering the electron density, and applying external magnetic fields. The following sections describes the physical background of each approach in turn. In the device described in Chapter 3, all these techniques have been incorporated. In the simulations in Chapter 4, all were simulated for, except for current application.

2.3.1 Confinement

Electrons excited to the conduction band in a semiconductor move randomly in all directions. However, when confining them to a narrow, or "quasi-1 dimensional" channel, the dephasing of spins moving in the confined direction can be much suppressed. With quasi-1 dimensional is meant that it has a width much smaller than the electron mean free path (the average distance an electron can travel without scattering) and precession length (the distance an electron covers before its spin had made one full precession), yet is much wider than quantum confinement lengthscales (when the confinement length becomes the same order as the particle wavelength, typically on the order of tens of nanometers). When electrons scatter back and forth in this confined direction, it can be seen from Figure 1(c) for the 2D case that the sign of the SO-field is inverted with each scattering, when the wavevector direction is *completely*

inverted. They will therefore have their spins precessing back and forth over a very small angle, and the average spin alignment will be roughly preserved. This effect, termed *motional narrowing* [13], is then a viable means for observing SDA in these quasi-1 dimensional wires in two dimensional electron populations in GaAs [10, 14].

An important main assumption in this confinement model is that scattering on the edges of the channel is specular, since this guarantees the constant flipping of the wavevector, and therefore the close repetition of the small spin precession back and forth, limiting spin dephasing. If the edges are rough, however, and each scattering gives a particle a random new direction, the SDA will be different [15].

In the case of a quasi-1 dimensional channel in bulk GaAs, the story becomes more complicated, since the scattering now takes place in *two* confined directions, and the Dresselhaus field has the more involved cubic form. Among other bulk effects, the consequences of this will be further investigated in depth in Chapter 4.

2.3.2 Passing current

When a current is passed through a wire as described in the previous section, the Fermi sphere (or circle) in k-space is shifted by an amount $\delta\vec{k} = -m^*\mu\vec{E}/\hbar$. Here m^* is the electron effective mass, μ is mobility, $\vec{E}$ is the electric field throughout across the wire, and $\hbar$ is the reduced Planck constant. This shift in k then directly implies a shift in the k-dependent SO-fields, given relations 2.1-2.3 [16]. Then performing Kerr rotation measurements on wires in different crystallographic directions, passing several different applied currents through each, can yield detailed information on the values of the SO prefactors. To faithfully extract these parameters, it is also necessary to have detailed knowledge of the exact values of the electric fields and mobilities in the wires. These values can be obtained seperately, by performing 4-point measurements on Hall bar geometries (more details on these 4-point measurements can be found in Section 3.3).

2.3.3 Gating

When applying a gate structure on top of a GaAs sample, applying gate voltages in the sample growth direction can alter the size of the Rashba field prefactor C_R, while leaving the size of the Dresselhaus prefactor C_{D3} relatively unchanged [16]. This is because of the dependency of C_R on the derivative of voltage over the electron population [17]:

$$C_R \sim < \psi | \frac{dV}{dz} | \psi >, \tag{2.4}$$

where V is the voltage over the spin population, and ψ is the electron wavefunction. The Dresselhaus prefactor does not have a similar dependency, since it is a bulk effect. It has been shown in GaAs devices containing a 2DEG that the Rashba field prefactor can be altered significantly by tuning with a gate, even up to a sign change, while indeed the Dresselhaus term remained constant [16].

2.3.4 Altering electron density

A final way in which the *relative* size of the Rashba and Dresselhaus fields can be changed is by altering the density of electrons excited to the conduction band. The electrons move with a certain Fermi k-vector, the magnitude of which is directly determined by the electron

density. In the case of a GaAs 2DEG electron population altering the electron density will not change much (though still enough for some fine tuning), since the dominant SO-terms are the Rashba field and linear Dresselhaus field, both of which are linear in $\vec{k}$. In bulk, however, the Dresselhaus term is cubically dependent on $\vec{k}$, and so altering the electron density significantly shifts the relative size of the Rashba and Dresselhaus SO-fields.

2.3.5 External magnetic fields

Though not a means of changing the relative size of the SO-fields, an external magnetic field does influence the SDA in two ways. Firstly, an external magnetic field linearly adds to the SO-fields in the treatment of spin precession, enhancing the angular frequencies. This will result in the electron spins precessing faster around the resulting total field, which can significantly change the Spin-Orbit symmetries, and has been used in previous experiments in our group to clearly separate the response from a 2DEG and bulk electron population [12]. Secondly, due to the Lorentz force, electrons in a bulk population will describe cyclotron orbits along the external field lines. This cyclotron motion essentially "groups together" particles with wavevectors of the same size into the same cyclotron orbits. This reduction of the amount of individual orbits can reduce the spin dephasing, since dephasing follows from particles following different orbits, and having their spins then precess at different rates. In the 2-dimensional case, external fields are applied parallel to the confinement direction, and so these electrons do not have their trajectories influenced, since the resulting Lorentz force points out of the confining plane. The simulations for bulk electron populations need to and do take these effects into account, and this will be returned to in detail in Chapter 4.

2.4 Measurement principle

The electron spins in question are to be both excited and probed using an optical technique relying on *Kerr rotations* [18]. For maximum resolution of SDA with respect to thermal spin fluctuations, the samples are first cooled to 4.2 Kelvin by means of liquid helium (Figure 2.2). By then sending in a short pulse of circularly polarized photons (carrying angular momentum $\hbar$ in the [001] direction) into the top few hundred nanometers of a GaAs sample (the make-up of which is described in Section 3.2), a large population of aligned spins (order of magnitude 10^{15}cm^{-3}) can be created in the material, but this density can be tuned by altering the pump laser intensity.

Having made an aligned spin population using this technique, another pulse of photons is quickly sent in, these being linearly polarized (the black arrows in Figure 2.2). The reflection properties of the free electrons aligned by the initial pulse are such, that the axis of polarization is rotated, by an amount proportional to the alignment of the spins. Therefore, by sending in a circular pump pulse, waiting a few picoseconds, and then sending a linear probe pulse, one can measure the decay of the spin ensemble in this wait time, and by doing several of these measurements with increasing waiting times, a time-resolved picture of spin dephasing is created. For more details on this set-up, please see [19].

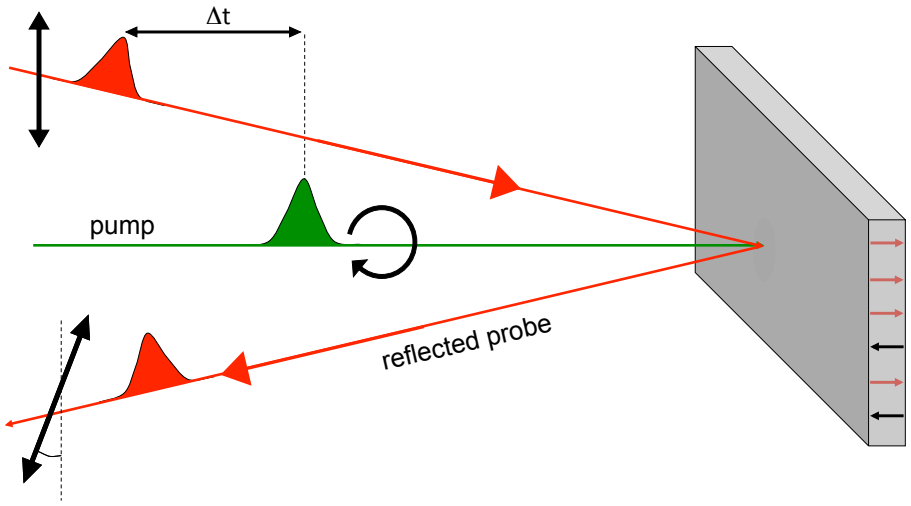

Figure 2.2: A cartoon depicting the principle off reflectance measurements on a spin population. The spin population is aligned perpendicularly to the surface by the circularly polarized pump. Then after Δt, a vertically polarized probing laser pulse is sent into the material, which will be reflected with a polarization rotation, linearly dependent on the remaining spin imbalance along the probe beam at the time of reflection.

Chapter 3

Device for measuring 2DEG and bulk SDA

3.1 Introduction

Previously in our group, measurements were performed on sets of wires in a sample of GaAs containing both a 2DEG, and a bulk layer with a Rashba-type SO-field [12]. However, this sample allowed for none of the tuning of the distinct SO-fields with respect to each other that were listed in Chapter 2, and so this part of the research is meant to be a natural extension of that previous work.

This chapter will be concerned with the design and fabrication of a device with which to measure SDA for both 2D and bulk electron spins in GaAs. In Section 3.2, the material properties are described. Next in Section 3.3, our methods for the realization of SDA manipulations from the theory chapter will be explained. Then in Section 3.4, the results from combining these features on the final device, together with any added constrictions, are discussed and presented. Since there are still some final fabrication steps left undone at this point, the results of testing for these steps are also presented here, so as to give as much of a complete understanding and appreciation of the final device as is possible, at this time of writing.

3.2 Device material properties

The wafer of GaAs we use is epitaxially grown, fabricated in the group of D. Reuter and A.D. Wieck, from the Ruhr-Universität, Bochum, Germany. Its bandstructure in the growth direction is illustrated in figure 3.1, with the different regions of interest indicated by capital letters. The left side is the sample surface. E_f indicates the Fermi level, E_c the conduction band, and E_v the valence band.

The layer sequence starts with bulk GaAs (A in Figure 3.1), with the [001] direction being the growth direction (note that this corresponds to the defined k_x- and k_y-dependence of the Rashba SO-field in Section 2.2). On this, a superlattice with ten periods of 5.2 nm GaAs and 10.6 nm AlAs is grown (B), to isolate the electron populations of the surface layers from the less pure material below. On top of this, 933 nm of undoped GaAs is grown (C), (the "accumulation layer" of electrons). This is followed by a 36.8 nm undoped spacer layer of

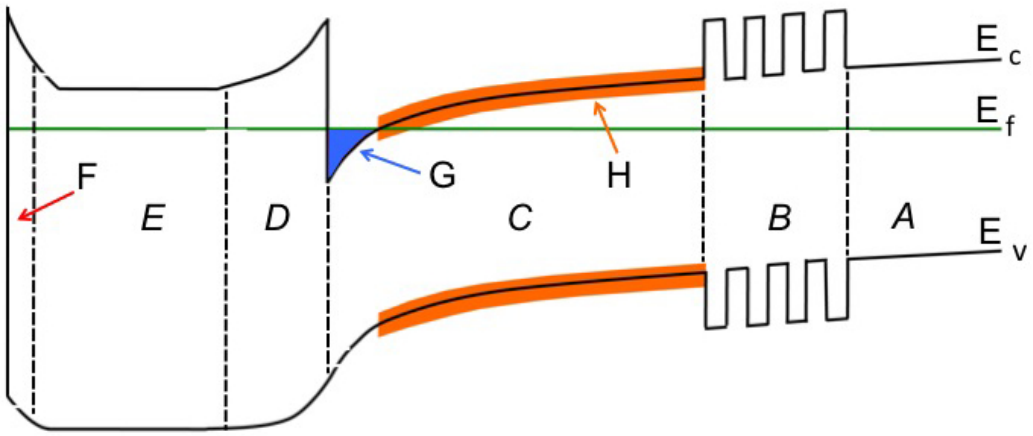

Figure 3.1: The bandstructure of our pristine GaAs samples (not to scale). The green line is the Fermi level, the red area is the 2DEG, and the orange area contains optically excited bulk electrons. Note that in the 2DEG there are always free electrons, while in the bulk region, these need to be excited there.

$Al_{0.32}Ga_{0.68}As$ (D). On top of this, al layer of 71.9 nm Si-doped $Al_{0.32}Ga_{0.68}As$ is grown (n-doped at 1 x 10^{18} cm^{-3}) (E). The sequence is then capped by 5 nm of GaAs (F).

As a result of this stacking, at around 100 nm from the surface the conduction band dips below the Fermi level (G). The reservoir created here is so thin in the growth direction (only a few nanometers), that the required wavevector to occupy a state in this direction is larger that any wavevector present in the reservoir, and so the electrons are quantum confined there, with a sheet density of around 10^{11} cm^{-2}. This region is therefore our 2DEG.

In the accumulation layer beyond this 2DEG, there is still significant band bending (H). Bacause of this, there will also be a Rashba-type SO-field here, experienced by electrons excited to the conduction band. These two distinct populations, 2DEG and bulk, will be probed simultaneously, something that can not be avoided given the optical measurement technique we use. Not all photons that reach the thin 2DEG are absorbed there and emitted back out again from there, even though the 2DEG contains many free electrons: some will pass through and probe the layers underneath the 2DEG, which contains our bulk population. These two populations dephase independently, and the signal from optical probing will contain dephasing information of these two simultaneously [12].

3.3 Realization of manipulating the SDA

3.3.1 Electron Beam Lithography

The several features we wish to implement in our device require several fabrication techniques (e.g. etching, evaporation, annealing), which differ per feature. One thing these fabrication steps have in common though is that the technique used to define *where* these features are to be realized is Electron Beam Lithography (EBL). To use this technique, the sample is first

cleaned *rigorously*. Then a layer of polymer resist is applied to the surface, and the sample is baked in an oven (for detailed recipe steps, see Appendix A).

The sample is then loaded into a vacuum chamber, where several identifiable points on the wafer (such as its corners, or pre-made structures) are identified by Scanning Electron Microscope. These points are used to map a drawing, made in a CAD-like program specifically written for the EBL, onto the sample (a simple mapping of the 3D coordinate space of the drawing onto the 3D space defined by the points just identified).

The polymer chains are then broken by an electron beam as defined by the drawing, and these broken-up parts of the polymer are washed off in a final development step. This leaves the sample masked and protected by polymer, except for where the sample is to be etched, evaporated onto, or otherwise. For the EBL-drawings used in the fabrication steps in the following sections, see Appendix C (digital, on CD).

3.3.2 Confinement

To create quasi-1 dimensional electron channels on this sample on which to measure SDA, the 2DEG- and bulk-containing GaAs needs to be removed where we wish to make our channel sides. To do this we employ a wet-etching technique, which isotropically eats into the material wherever it is exposed. At these places hydrogen peroxide first oxidizes the material, and this oxide is then removed by sulphuric acid (for recipe details see appendix A). This will remove material, isotropically, at a rate of around 2 nm per second, and this etching is done to a depth of around 100 nm. In Figure 3.2 the resulting distinction in bandstructure between etched and non-etched wafer is shown.

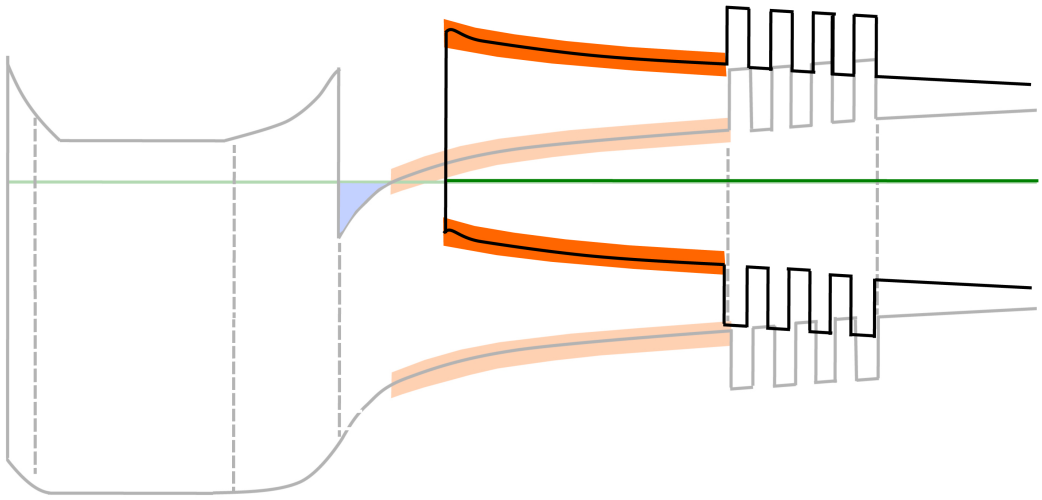

Figure 3.2: The bandstructure (not to scale) of a region that has been etched to 100 nm depth. When compared to the band structure for a pristine wafer (opaque in this figure), it can be seen that bulk free electrons in a pristine wafer are isolated from the etched regions, even though the etching does not physically remove the neighbouring material, because the conduction band is significantly higher there.

In the etched region at the sample surface, a Shottky barrier is formed due to surface effects.

Because of this, there is still some band bending left in the bulk region, and therefore there are also still Rashba SO-fields. However, even though we have not etched away the entire layer of GaAs containing the bulk layer, the disappearance of the highly doped region at the surface ensures that the etched region conduction band is of much higher energy than that in the unetched regions. Therefore, the bulk free electrons are trapped in the unetched regions. Also, when etching to this depth, the free electrons in the 2DEG can clearly not move outside of the unetched regions, since there is simply no GaAs left there. So effectively, by etching away material to a depth of 100 nm, both 2DEG and bulk spin populations are confined to whatever shape is etched around.

To avoid confusion: the 2DEG region naturally contains many free electrons, but the bulk region has almost none in comparison, in equilibrium. When talking about electrons moving through the material, we necessarily mean free electrons, which are excited by an initial optical pulse as described in Section 2.4. All results in this thesis are therefore on 2DEG and bulk excited population physics.

3.3.3 Passing current

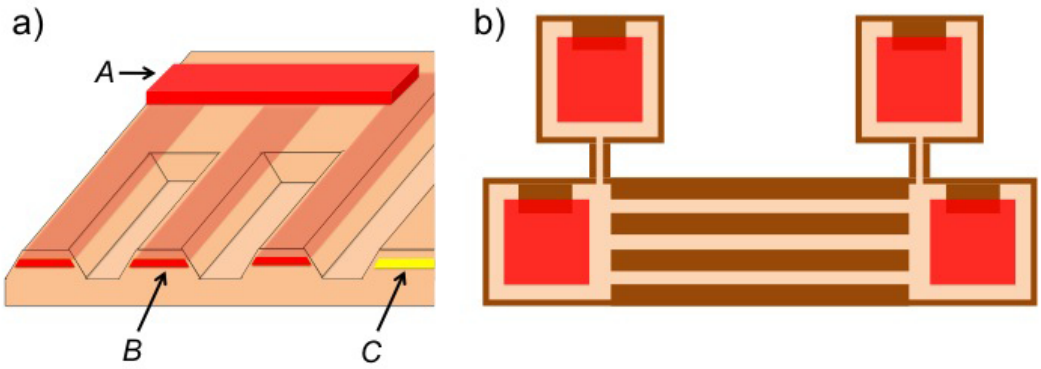

Figure 3.3: a) 3D cartoon of the ohmic contact contacting the 2DEG. The red block is an ohmic contact, and the red stripes are 2DEG that has been contacted. The channels have been seperated by etching, and the yellow 2DEG to the side has been completely isolated from the ohmic.
b) Cartoon illustration of the top view of the required 4-point measurement setup. Between the left and right ohmics (red) a current is passed, through 2DEG wires (light) defined by (dark) etching. The upper two ohmics (red) are then connected through 1 μm wide openings to the current path, where they can probe the voltage drop over the wires. The whole arrangement is seperated from its surroundings by etching, and guides are etched into the GaAs to force edge state electrons to enter the region connected by the contacts.

For sending electrons through the wires described in the previous subsection, we need to contact the 2DEG through the surface of the material. For this, a recipe has been previously established in our group [20]. This recipe consists of first evaporating 120 nm of gold-germanium, then 30 nm of nickel, and topping it with 20 nm of gold. This stack of metals is then annealed at 450 degrees Centigrade, so that it forms a melt that diffuses down into the GaAs. The rate of diffusion is steady, and so this metallic contact can be aimed

precisely into the 2DEG, forming an ohmic contact with a resistance of, in our case of 200 x 200 μm^2 contacts, as little as 100 Ω at liquid Helium temperature. A cartoon representation of such contacts (with a view inside the etched sample, as if cut by the page) is shown in Figure 3.3(a), with the ohmic contact labeled A, the contacted 2DEG labeled B, and the non-contacted 2DEG labeled C. A current can then be sent into one contact, through the 2DEG, and extracted from another contact, while the voltage drops over wires or unetched pieces of wafer can be probed by additional ohmic contacts along the current path. To define such current paths, and make sure the places along this path where the voltages are probed are well-defined, more etching is required. This is illustrated in Figures 3.3(a), where the 2DEG labeled C is separated from the ohmic contact, and Figure 3.3(b), showing a schematic top view of such a configuration with the ohmics again in red, contacting 2DEG which is colored light, bordered by etched material colored dark. A final touch is required here though, since we also wish to measure under external magnetic fields. Electrons caught in edge states in the unetched material, skipping with tiny cyclotron half-orbits in an external field, must be led into the ohmic contacts by guides, visible in Figure 3.3(b), running into the sides of the ohmic contacts.

3.3.4 Gating

To be able to perform optical measurements on the sample, the top gates lying on the wires need to be transparant to the frequency of light that will be used in the Kerr rotation measurements. In our group, previous research has gone into such transparant top gates. The chosen materials were SiO_2 as the insulator, and indium-tin-oxide (ITO) as the transparant metal-like glass on top of the insulator. Both are sputtered onto the material (for recipe details see appendix A, or the bachelor thesis by Z. H. Sainz [21]).

Most importantly for such a gate, there must be no leakage, since this would send a current through our wafer (albeit a small one), and this (as shown in Section 2.3.3) would change the SO-parameters. To nullify the chances of leakage, there may be no holes in the SiO_2, and there may be no ITO reaching over the insulator and contacting the GaAs surface.

Of course, a second contact is needed either at the back of or inside the device, to apply a gate voltage over the device in the [001] direction. For this, one more ohmic contact is used that contacts the 2DEG, allowing us to set a voltage of several volts over just 100 nm of material, causing significant changes in the band structure, and thereby the Rashba SO-field.

3.4 Results

This Section will discuss the actual device that incorporates all the features discussed before, for as far as it has been completed thus far. The fabrication steps are listed in sequence. First, etching is discussed, then evaporating ohmic contacts, and finally sputtering gates.

3.4.1 Wires

When wishing to combine the features described in the previous section onto a device, some additional things must be taken into consideration. First of these is the fact that we wish to probe only regions that will exhibit SDA in a confinement, which would require only a single channel. However, a single wire can not be uniquely probed, since the minimum diameter we can reduce our Kerr laser spot size to is around 100 μm, and the resulting total signal would only contain a very small contribution from the region that would exhibit SDA. Therefore, we create regions of 200 μm 200 μm to measure on by putting 125 channels together of 200 μm length, 1 μm width, and 1.6 μm periodicity. To avoid confusion, we will from here on refer to such a square as a *set* of wires.

Etching such a set of wires can sporadically (partly) fail, since etching micron-sized structures is a very fragile procedure, dependent on extreme cleanliness of the sample. Therefore, some redundancy is advisable, making three sets of channels for every direction we wish to measure in. To image such small wires, we use a Scanning Electron Microscope (SEM), a basic tool for nanofabrication analysis, that allows imaging of very small structures by probing a surface with electrons of very short wavelength. Figure 3.4 shows an examplary picture taken by SEM of a wire set we were able to fabricate.

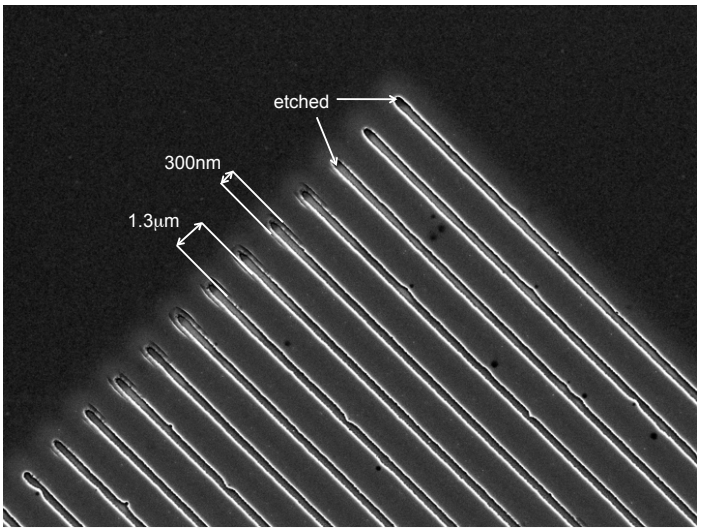

Figure 3.4: Scanning Electron Microscope image of a corner of a square of wires, showing very few etching faults due to contaminants. Distances as indicated.

The wet etching of micron-sized structures being such a fragile procedure, every step that precedes it brings additional risk of sample contamination. Presence of particles from cutting of the wafer, particles that come from the sides because of handling with tweezers, remaining polymer, and anything else that makes the sample less than pristine will ruin etching results. Because of this we have made etching the very first step in our fabrication process. And, since all following fabrication steps need to be aligned for EBL with the etched structures, we also etch a number of markers onto the outer, unused areas of the piece of wafer we use. The etching has a final restriction on the device, and that is that the polymer mask needs to be homogeneously thick. When applying a polymer mask for EBL, it tends to become thicker nearer the edges, so there needs to be at least a millimeter between the outermost, micron-sized etched structures and the sample edge (in this outer border, the just mentioned significantly larger marker structures can still be properly made though).

Added to these demands, the maximum size of the final device, which must fit onto the chip holder of the Kerr rotation measurement setup, is 2.5 mm by 4 mm. It was decided, for some redundancy and so as not to waste too much expensive 2DEG containing wafer when making multiple devices, to place two identical final device designs on a single sample, side by side. After all fabrication is finished, these need to be seperated by cleaving the sample, and also the 1 mm boundaries need to be removed. The etched sample resulting from all these demands is shown in Figure 3.5.

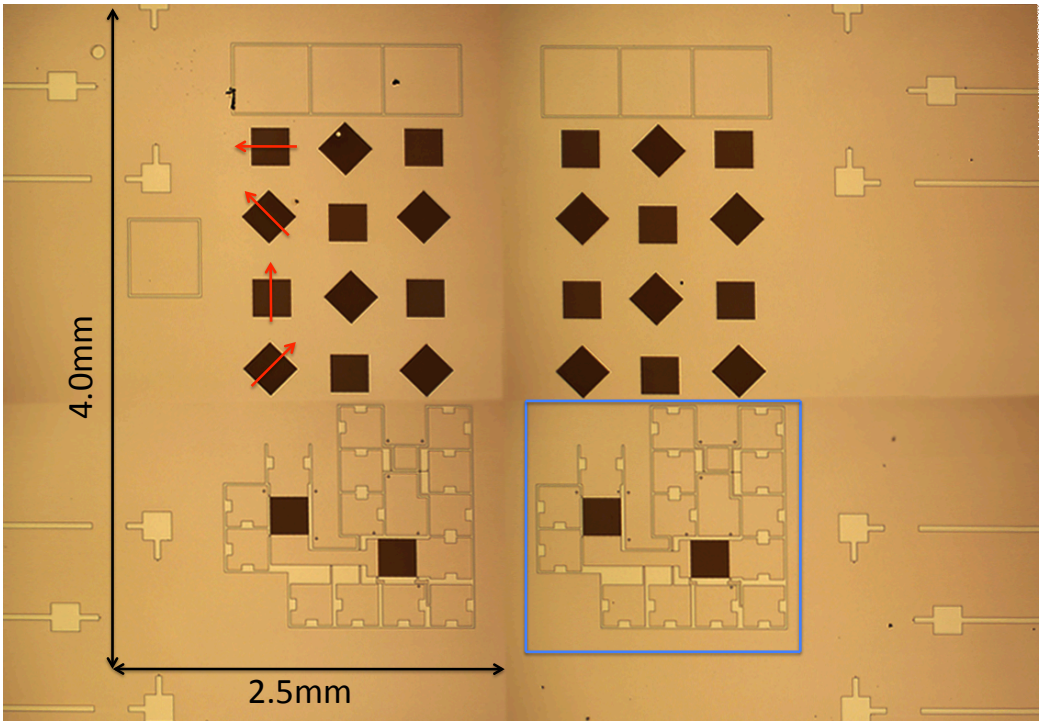

Figure 3.5: An etched sample of 7 mm by 6 mm, with the final device of 4 mm by 2.5 mm outlined by two black arrows. All closed shapes are etched, the darker areas are sets of wires. Vertically, consecutive wires run in different directions, as indicated by the red arrows drawn through the four left most sets (all 5 vertical rows of 4 sets of wires, to the red arrows' right, also contain all four wire orientations). The larger triple boxes above the wires serve to bond the gates are used for the top gates (explained in subsection 3.3.4). The structures just below the wires, enclosed in a blue drawn box, are used for the measurements involving current (explained in subsection 3.3.3). The remaining etched shapes, nearest the sample edge, are lithography alignment markers.

3.4.2 Etching for current measurements

Besides device dimensions, the chip holder has another constriction to add to the measurements involving current, namely that it can only accomodate up to 12 electrical contacts for measurements at a time. Adding up (the to-be-contacted metallic pads are numbered in the same way in figure 3.6, with not-yet-fabricated ohmics drawn in), we need three contacts for the gates (1-3) (why this is will be explained in subsection 3.3.4), two contacts for passing a current (4,5), and two contacts for measuring voltage drops for every set of wires we pass current through, of which we have two (6-9). We also wish to be able to measure longitudinal and transverse resistivity and mobility, for reference, on an unpatterned area where current is passed through, and for this we use the remaining three contacts (10-12). These are the main contacts to be used.

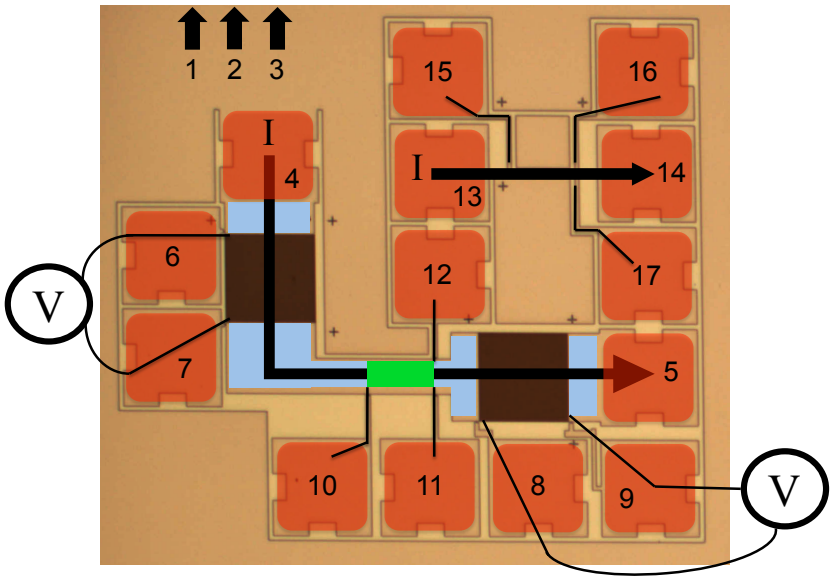

Figure 3.6: Zoomed-in current measurement area on the device from the blue box in Figure 3.5, with not-yet fabricated ohmics drawn in red. The blue represents the main current path between ohmics 4 and 5, with the black arrow representing the current. Ohmics 6 and 7 measure the voltage drop over the vertical wires, ohmics 8 and 9 measure the voltage drop over the horizontal wires. Ohmics 10, 11 and 12 measure voltage drops over the green unpatterned, unetched area where the current passes. Between ohmics 13 and 14 current can be passed through a single wire, wich is then probed by ohmics 15, 16 and 17. 1,2 and 3 point up out of the figure, where the three remaining contacts are made for the top gates. Ohmic 4 also doubles as a ground for the 2DEG.

However, if for example needed for reference, it might be fortuitous to be able to perform these reference measurements on a single wire (even though the laser spot can not be focussed on this wire alone), through which a seperate current can be passed (13,14) and probed (15-17). These measurements can not be connected to the chip holder at the same time as the other measurements, and will so require some extra effort to be used, in a seperate cooldown.

3.4.3 Etching for top gates

For the gating, it is advisable not to use one big single top gate: if there is a single leak, using the gate guarantees there will be an unwanted current flowing through the device altering experimental conditions somewhere. Thus, splitting up the required gate into different segments, each covering different sets of channels and operable independently of the others, is desirable. Also, the gates should not cover any ohmics.

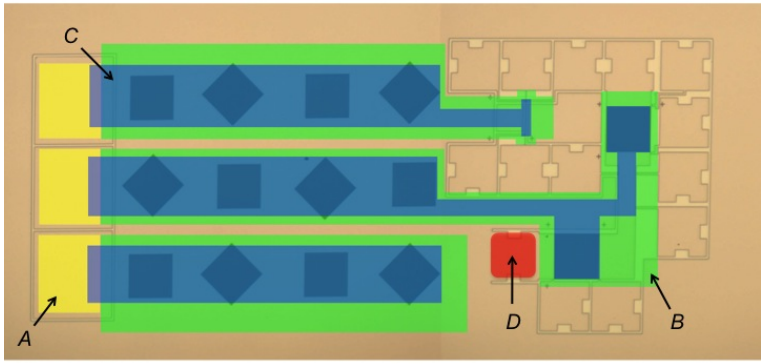

Figure 3.7: The final device of 4 mm by 2.5 mm, rotated 90 degrees from Figure 3.5, with the intended gates and bond pads drawn in, in color. The yellow squares (A) are the bond pads of Ti:Au, isolated in the etched squared to the left of the wires. The green (B) is SiO_2, the blue (C) the ITO on top of that. The lower top gate only gates the lower four sets of wires, the middle top gate gates the middle sets of wires, and both sets of wires in the current measurement area, and the upper top gate gates the last four sets of wires, and the single wire. The red ohmic (D) is also used to ground the 2DEG.

To further reduce the risk of gates leaking, we add metallic pads (Ti:Au) to the device, seperated from the electron populations we wish to measure on by etching material away around the pads (i.e. creating a mesa-structure), which are connected to the ITO. The micrometer-scale wire-bond contacts used to connect a voltage source to the ITO are then connected to these pads, to avoid the risk of sticking these right through both ITO and SiO_2. These bond pads are also much easier to reliably bond to than the hard, glassy ITO. Top gate designs (yet to be fabricated) that meet all these demands are shown in Figure 3.7. Notice that each gate covers one set of wires in each crystallographic direction.

3.4.4 Ohmic contacts

After the etching step that has been thoroughly illustrated in the previous sections, this current research hit a wall that could not be climbed within the alotted time of a master project. However tests were done to establish exact and reliable recipes, before submitting the etched samples to further fabrication steps. Those results are presented here.

Although there have been many publications about the recipe for ohmic contacts we wish to use, both from our group and from others, an unknown problem presented itself while attempting it, seen in figure 3.8(a). After evaporating the intended metals onto the sample, covered with polymer mask except for where the ohmics should go, lifting off the superfluous metal results in lifting off of *all* metal film, and the ohmics are destroyed. Clearly, the metal is not sticking well to our GaAs substrate.

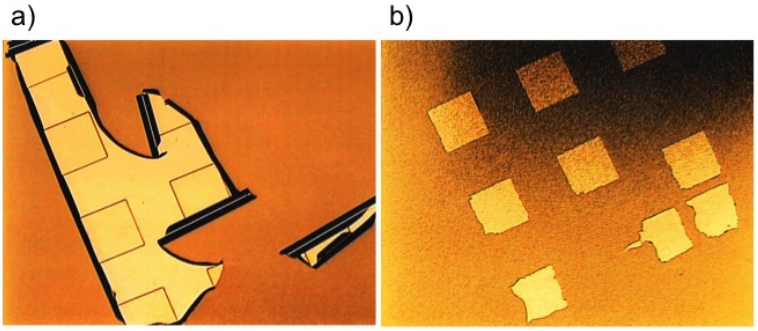

Figure 3.8: a) The squares visible on the yellow flakes (200 μm^2) are where the ohmics should be located, fabricated by the recipe used earlier, and with succes, in our group [22]. Clearly, the lift-off of the deposited metals destroys the intended ohmic contacts.
b) Ohmic contacts after aggressive ultrasonic bath lift-off, when a 1 nm layer of titanium was added to the conventional recipe, between substrate and contact metals.

The cause for this has been sought in a number of things (evaporated metals, sample cleanliness, which evaporator was used, oxygen etching, evaporation rate, temperature, not using an ultrasonic bath), but the metal kept lifting off. Eventually, a very thin sticking layer of titanium (1 nm) was introduced, which should keep the metals in place, but still be porous enough to allow the metals to diffuse past it, forming the desired ohmic contact. The result of this is seen in figure 3.8(b). While clearly the metals stick better than without titanium, they are still not the simple squares they should be. They also seem to stick better on the darker, rougher surface, which is from the edge of the original wafer, with the black spots coming from arsenide depletion.

Continuing the device fabrication, it will be very important to check the resistance of ohmic contacts made with this titanium layer (or, to discover what causes the bad sticking properties in the first place). If the titanium-enhanced contacts are found to be good, an optimum could be sought for, between titanium thickness (and therefore even better sticking) and contact resistance.

3.4.5 Top gates

As mentioned in Section 3.3.4, research on transparant gates has already been performed in our group, and from this research came requirements on growth and required thickness of the two seperate layers. However, these layers were grown on a sample using a mechanical mask (a covering piece of metal with holes in it), which gives too little control over the placement of the gates of the final design. To have micrometer control over this, we need to use a polymer mask, as described in section 3.3.1. The added difficulty will then be lifting off the hard, glassy SiO_2 and ITO.

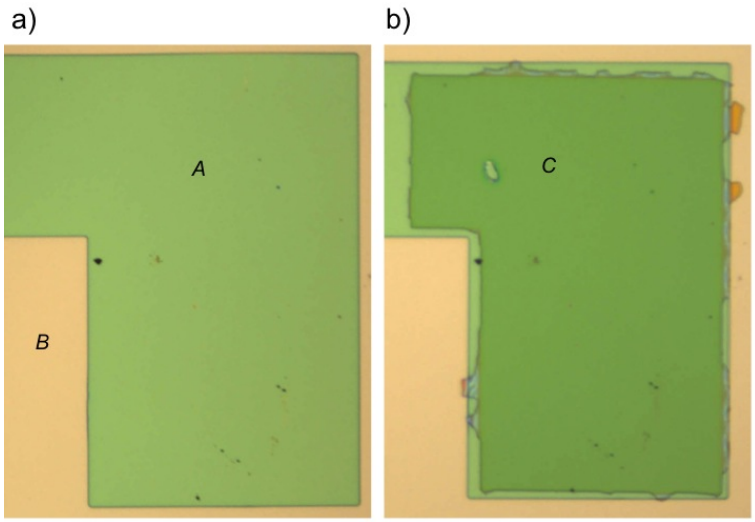

Figure 3.9: a) SiO_2 (green), on substrate, after aggressive ultrasonic bath lift-off. b) ITO (darker green) deposited on this SiO_2. Some jagged edges can be seen, of lengths up to around 50μm.

Figure 3.9(a) shows the result of lift-off for a layer of SiO_2, which looks good enough for our purposes, and Figure 3.9(b) shows the same for ITO deposited on top of this SiO_2 layer, which looks worse. Clearly, the gate in Figure 3.9(b) would leak, since the metallic glass is reaching over the edge of the insulator. Apparently, ITO, despite being twice as thin a layer as te SiO_2, is harder to remove.

As a remedy to this, the margins (20 μm in the above design) need to be made larger, and an additional test of this is desirable. This single sample is of course not a basis for statistics, but along the entire edge of the ITO, the maximum protrusion from the desired profile is some 50 μm, so that is what should be the minimal margin between the edge of the SiO_2 and the metallic ITO on top of it, and preferably more (as much as can be reasonably fitted on the device). Aside from margins, any sharp corners in the design should be avoided as much as possible, since it appears the lift-off goes harder there.

3.5 Conclusions

A device was designed to measure SDA properties on bulk and 2DEG electron spin populations in GaAs, under influence of currents passed through the material, orientation of etched constrictions in certain crystallographic directions, external magnetic fields, and top gates. The necessary fabrication steps of etching, ohmic contacts and top gates have been calibrated, and of these the etching has been perfected. Some few tests are advised before finishing the final device, tests for which this master project didn't allow time anymore.

Chapter 4

Numerical experiments

4.1 Introduction

This chapter will detail efforts to simulate SDA in bulk populations, where the threedimensional cubic Dresselhaus SO-term is present, and can be of equal magnitude as the Rashba term. Also the effects of external magnetic fields will be taken into account, which will cause the electrons to follow cyclotron orbits. These effects combine to significantly complicate the picture of motional narrowing given in Chapter 2, which served to explain SDA in 2DEG spin populations. First, in Section 4.2, the workings of the simulation are explained. Then, in Section 4.3, we will go through the results for simulations with zero external field, vary the electron density, change the SO-parameters with respect to each other, and then turn on the external field.

4.2 Method

The numerical approach is based on a semi-classical picture for the electron motion in the material. Electrons are assumed to move with Fermi velocity (independent of the momentum direction). They never escape the region of the interest as they scatter on the walls elastically. For smooth walls this will be specular scattering, while elastic scattering on a wall with significant surface roughness is modeled as elastic scattering in a random direction (non-specular). Electrons also have a probability to scatter inside the volume of interest, which is defined by the mobility. This approximation for electron motion is valid for motion in directions without quantum confinement, and for the case of $E_F \gg kT, \Delta E_{Zeeman}, E_{SO}$. For a more detailed explanation of this approach, please refer to previous work in our group [20, 14, 19]. These works (and related results from the Folk group [15, 23]) on modeling the spin dynamics in confined structures of material with a two-dimensional electron system showed that this approach is reliable and efficient.

Here the focus lies on modeling the temporal evolution of spin polarization in a three-dimensional electron ensemble that is ballistically confined in a wire (typical dimensions are 1 μm wide by 1 μm deep by 200 μm long). The total SO field that electrons experience consists of the bulk Dresselhaus term (Equation 2.2) and the Rashba term (Equation 2.1). Inclusion of the bulk Dresselhaus term is natural, while the Rashba term for three-dimensional structures is rarely considered. Nevertheless a Rashba-like SO field also appears for structures without a pure two-dimensional nature, since the necessary requirement for heaving such SO

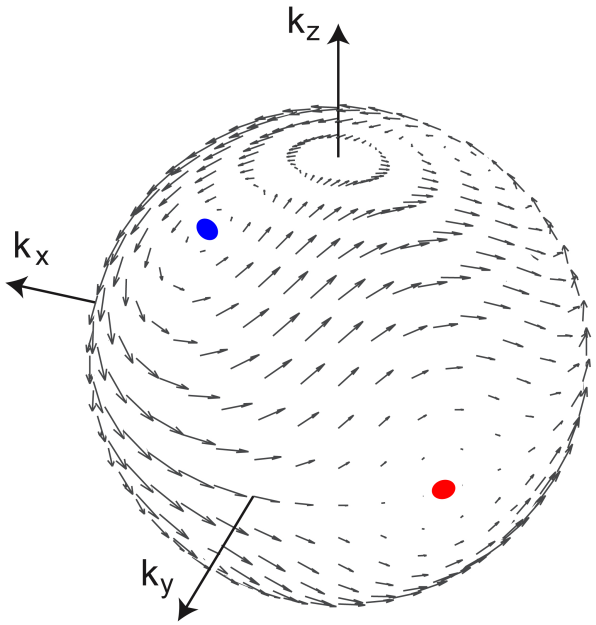

Figure 4.1: The total spin-orbit fields experienced by electrons with the Fermi velocity in bulk, for when $|\vec{B}_R|_{max} = |\vec{B}_D^{bulk}|_{max}$. This leads to $B_{SO}^{total} = 0$ for electrons that move in $[\bar{1}10]$ and $[1\bar{1}0]$ direction (red), and for some directions with non-zero k_z (blue).

present is hidden in the asymmetry of the potential. A Rashba term should be effective in all cases with a unidirectional electric field in the volume of interest.

In this case of epitaxially grown GaAs, exact cancellation of SO-terms is also still possible for specific directions of electron motion. The potential advantage of using three-dimensional structures lies in the possibility of strongly tuning the cancelation of Rashba and Dresselhaus terms by tuning the electron density (which is easy to achieve for the optical experiments in which spin dephasing anisotropy (SDA) was observed [12]). It comes from the fact that B_D is proportional to k^3, while the B_R is linear in k, and the value of k_F in the system is defined by the total electron density. An example of the engineered cancelation of SO field is presented in Figure 4.1.

For the case with no external magnetic field the modeling of such a three-dimensional wire is not very much different from the two-dimensional case. However, the presence of such a field with a magnitude that is of interest in the experiments requires inclusion of the cyclotron motion of an electron (the SO-fields do not contribute significantly to any Lorentz motion, since the SO-fields and particle velocity do not exist simultaneously in the same frame of reference). At the same time, the calculation should keep track of the spin precession in the total field (external plus SO fields), and account for momentum scattering on the walls of the wire. This extension thus makes the calculations for the 3D case computationally much more demanding than the 2D case. However, the simplicity of this numerical approach on a complex physical situation still counts as a significant advantage in comparison with efforts that aim at analytically solving this model.

A necessary requirement for observing SDA in three-dimensional wire is (as for the 2D case) that the spin precession length is smaller than the transverse wire dimension. For these

simulations the material parameters were kept at values that yield a spin precession length of about 10 μm in zero external field. In the numerical experiments the wire orientation is varied in the xy-plane. This is the primary parameter in the search for SDA, that should appear as T_2^* values that depend on wire orientation. Also, the electron density, strength of the coupling parameter for the Rasba SO, and the value of the external magnetic field are varied.

4.3 Results

The expectation was to find non-zero SDA results for 3D wires (based on extrapolating such findings for the 2D case) that would show a maximum T_2^* for a wire orientation along the direction with the smallest SO fields (all in the xy-plane, see Figure 4.2(b)). A wire orientation perpendicular to this direction should then give a minimum T_2^*. For cancelation of B_D by a B_R term as in Figure 4.2(b) this would lead to a maximum T_2^* for wires along the $[\bar{1}10]$ direction, and minimum T_2^* for the [110] orientation. However, while Figure 4.2(b) represents the magnitude and sign for the sum of B_D and B_R that serves as a reasonable estimate for the experimental situation, the expected SDA is then in fact *opposite* to what was observed in the experiments [12] (both 2D and 3D wires had a peak in T_2^* for wires in the [110] direction). This discrepancy is further explored in Section 4.3.1.

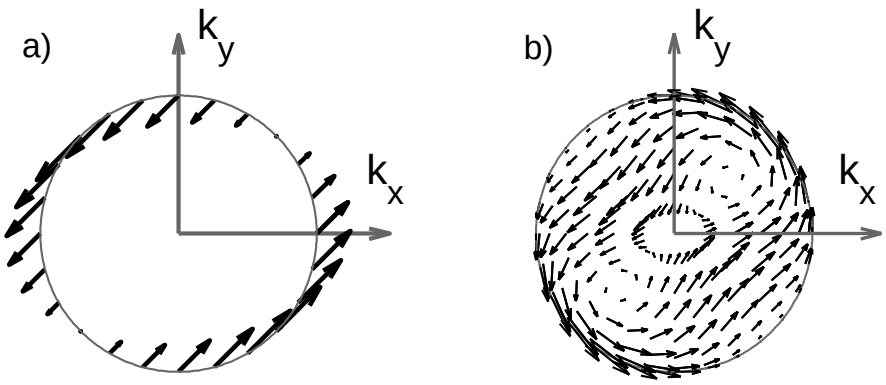

Figure 4.2: (a) A schematic representation of the SO-fields as an effective magnetic field for selected points (Fermi circle with radius k_F in the k_xk_y-plane) in two-dimensional k-space. The SO-field is the sum of the Rashba field and linear Dresselhaus field for the two-dimensional case with exact cancelation for k-vectors in [110] direction. (b) A similar representation for selected points in three-dimensional k-space (top view onto a Fermi sphere with radius k_F), with the total field as the sum of the Rashba field and the bulk (cubic) Dresselhaus field for the three-dimensional case. Both the magnitude and direction of the total SO field are depicted as arrows. For the 2D and 3D case the Rashba term has the same sign, while the Dresselhaus SO field has its sign inverted in the k_xk_y-plane. This sign flip is due to the fact that for the 2D case $\langle k_z^2 \rangle \gg k_x^2 + k_y^2$, while the dominant motion in the xy-plane for the 3D case is carried by electrons with $k_z \approx 0$ and $k_z^2 \approx 0$.

Note that in the three-dimensional case the direction of the SO-field cancelation is opposite to that of the two-dimensional case (Figure 4.2) if the focus is only on motion in the xy-plane. This comparison is for identical signs for the underlying Dresselhaus and Rashba terms, but the symmetry changes because the effective sign for the Dresselhaus contribution gets reversed (see Equations 2.2 and 2.3, for the 2D case $\langle k_z \rangle = 0$ and $\langle k_z^2 \rangle \gg k_x^2 + k_y^2$, while the dominant motion in the xy plane for the 3D case is carried by electrons with $k_z \approx 0$ and $k_z^2 \approx 0$).

4.3.1 Results for zero external magnetic field

The discussion of results starts with the simulations for zero external magnetic field. Here the electrons move randomly in the wire and experience specular scattering on the edges and random scattering inside the wire. The spin ensemble is prepared in a state that points in the [001] direction.

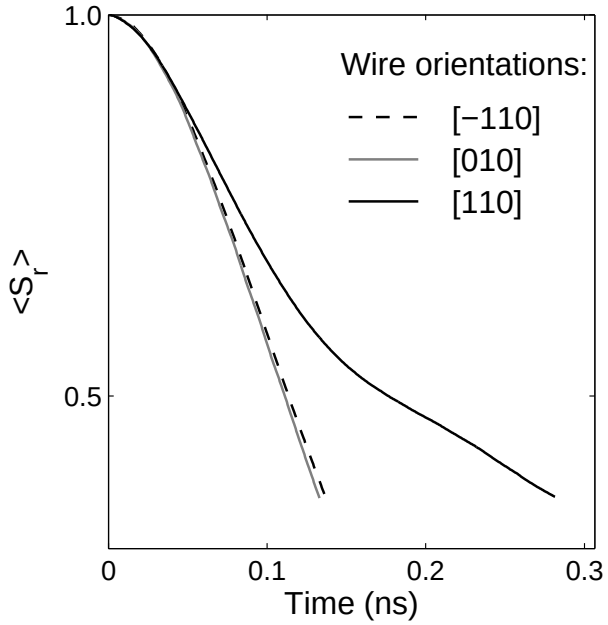

Figure 4.3: Ensemble spin expectation value $\langle S_r \rangle$ as a function of time for different wire orientations.

Calculated time traces with the expectation value for spin polarization in the ensemble are presented in Figure 4.3. Here $\langle S_r \rangle$ is shown (spin expectation value in the direction that it is maximum) to account for collective spin precession, but for this plot it overlaps with results for $\langle S_z \rangle$. The spin expectation value for an ensemble decays in time due to precessional dephasing in the SO fields. For wires along the [110] direction the spin dephasing is clearly suppressed in comparison with wires in the other directions.

T_2^* values were calculated for a range of wire orientations (Figure 4.4(a)). The wire direction [110] yields the slowest spin dephasing for an electron spin ensemble. Notably, this is consistent with the experimental observations [12], but opposite to our qualitative expectation that the directions on the Fermi sphere with near-zero SO fields determine the direction in which wires give the longest T_2^* values (as for the 2D case). Thus, this qualitative argument can not

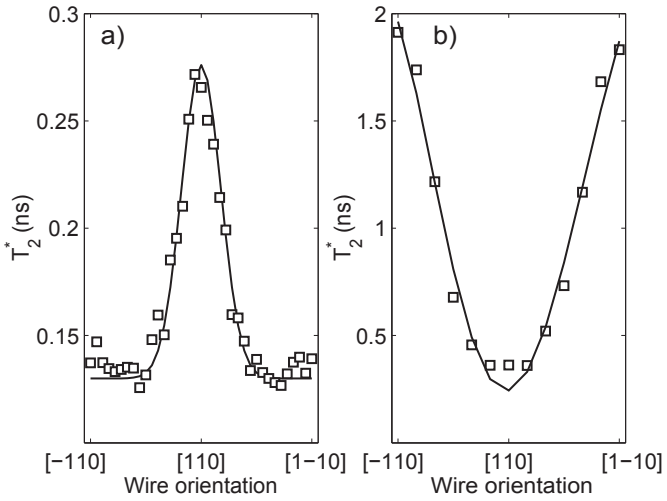

Figure 4.4: The spin-dephasing time T_2^* of a spin ensemble plotted as a function of the wire orientation. (a) For electrons with specular momentum scattering on the edges of the wire. (b) For electrons with non-specular momentum scattering on the edges of the wire.

explain the results for the 3D case.

To make a connection to the standard motional narrowing picture [13] the scattering on the edges of the wire was changed to non-specular (i.e. scattering in a random direction). Results for this case are presented in Figure 4.4(b). For those boundary conditions, the simulations *do* give the longest T_2^* values for wires in the $[\bar{1}10]$ direction, and minimal values for [110] oriented wires. These results are indeed consistent with the motional narrowing mechanism, and simply show the longest T_2^* for the wire direction where the spin-orbit field is the smallest for electron motion along the wire (and vice versa): dephasing from having the highest SO-field values from motion transverse to the wire direction is suppressed by frequent momentum scattering on the walls. This dependence on scattering mechanism is a novel 3D feature: it has been shown not to be there in 2DEG spin populations [20].

An additional check that was performed is for specular scattering for a wire with transverse dimensions of 0.7 μm by 1.4 μm. This gave results very close to the SDA as for specular scattering in the wire with 1 μm by 1 μm transverse dimensions. Further, it was checked that setting the Rashba term to zero for the case of specular scattering gave $T_2^* \approx 0.33$ ns, with almost no dependence on wire orientation.

Comparing the different cases, it can be concluded that, for the case of specular scattering, SDA in bulk is not due to the confinement enhanced motional-narrowing effect, prevalent in 2D. Instead, the SDA must be due to an interplay between repetitive ballistic electron trajectories in the wire (from frequent wall collisions), and the complex anisotropy in the spin orbit fields. This mechanism for specular scattering has similarities with the phenomenon of ballistic spin resonance, which has been shown to also occur in wires based on 2D electron systems [24]. However, here it can already occur when the width of the wire is well below the spin precession length, unique to 3D.

Clearly, the scattering symmetries are more important in 3D than in 2D populations, since a far larger fraction of possible electron paths leads a particle into a boundary of the wire

instead of along the wire, since the directions of motion are equally distributed over the Fermi sphere, instead of a circle. Attempts were made to identify SO-field symmetries, responsible for the unexpected results. However, calculating the (vector) sum of the fields that a particle experiences when traversing several simple symmetrical paths in a wire, as a function of wire orientation, yielded no significant results. Of course, for a more complete analysis, the angle of the field with respect to the (initially aligned) particle spin should be taken into account, and distributions and weights introduced. This analysis quickly becomes very cumbersome, and a Monte Carlo analysis becomes a better approach.

Since the scattering mechanism for wire edges in the real devices is more likely to be specular (due to screening, the potential a the edges is smoothed) we further focus only on this type of the scattering.

It is now useful to attribute a numerical value to the SDA. For the following results, it is defined as the ratio between the spin dephasing time in a wire along the [110] direction and a wire along the $[\bar{1}10]$ direction.

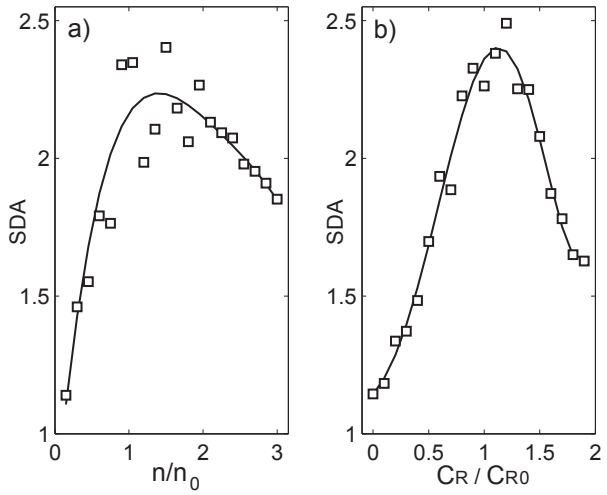

Figure 4.5: Spin dephasing anisotropy SDA as a function of simulation parameters. Data points from the numerical experiments are supported by a guide to the eye (solid line). (a) Electron density dependence of the SDA. (b) Dependence of SDA on the relative strength of the Rasha SO field (normalized to the value which yields $|B_R| = |B_D^{bulk}|$ in the xy-plane).

To next investigate the link between the SDA and exact cancelation of the SO field along the direction perpendicular to the wire, two simulation parameters were varied. Results from varying the density of electrons (and thereby k_F) in the wire are presented in Figure 4.5(a). It shows a clear maximum SDA for the value of the electron density which leads to exactly zero SO field in the direction $[\bar{1}10]$. This provides further evidence that the symmetry of the SO fields indeed underlie the SDA. This is further confirmed by results for the SDA as a function of the strength of the Rasha spin-orbit coupling, shown in Figure 4.5(b)), where the SDA displays similar behavior as in Figure 4.5(a). The SDA weakens when deviating from values which give exact cancelation of the two SO fields for electrons with k-vectors in the $[\bar{1}10]$ direction.

4.3.2 Magnetic field dependence

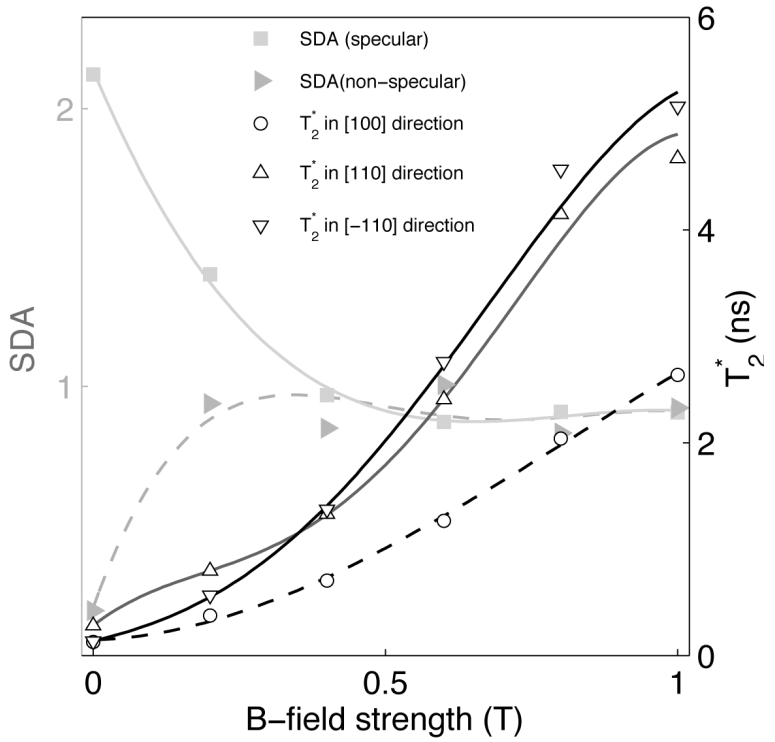

Figure 4.6: Against the right axis, the T_2^* values for wires oriented in [100], [110] and [$\bar{1}$10] are shown as functions of magnetic field in the [100] direction, for specular scattering. Against the left axis, the resulting SDA is plotted (squares), defined as before. The SDA that results from cancellation of the internal SO-fields can be clearly seen to disappear for magnetic fields of around 0.5 Tesla. Also the SDA for the non-specular scattering case is plotted (filled triangles), and here, all trace of SDA resulting from internal SO-fields has already disappeared when the external field becomes larger than 0.2 Tesla.

To include the external field, one has to take two contributions into account: spin precession in the total magnetic field experienced by the spin, and the external field's influence on the motion of the electrons. The first can be easily achieved by adding a constant vector to the spin-orbit term experienced by the electron spin, while for the second contribution more involved analysis is required. The electrons now follow cyclotron orbits in between scattering events, complicating their orbits, and hence also the SO-precession. This part of the simulation is computationwise the heaviest.The results for ensemble dephasing in an external magnetic field in the [100]-direction are presented in Figure 4.6, with B varying from 0 to 1 Tesla, and Figure 4.7, for fixed external fields of 4 and 6 Tesla.

Firstly, the rise of dephasing times and the change in orientation dependency can be seen in Figure 4.6. Clearly, as can be seen from the right T_2^* data, the dephasing times in all directions rise when an external field increases from 0 to 1 Tesla. Also the SDA, as seen on the left axis (and still defined from the zero-field case as the fraction of T_2^* in the [110] and [$\bar{1}$10] directions), disappears for external fields with a strength of not even 0.5 Tesla, as the magnitude of the dephasing times becomes much larger than any difference between them in

these directions. Such a decay to 1 of SDA between the [110]- and [$\bar{1}$10]-directions has also been reported in experiments in our group [12].

Also shown in Figure 4.6 is T_2^* for the wire oriented along the magnetic field, which rises much more slowly with magnetic field. From this abberant behaviour, we can conclude that we can no longer assume the SDA characteristic to be a single, fully symmetrical peak around one wire orientation, when the external magnetic field becomes comparable to and larger than the SO-field. In this case, the external field will dominate the shape of the SDA, as a function of wire orientation. The shape of such an SDA profile will be discussed next.

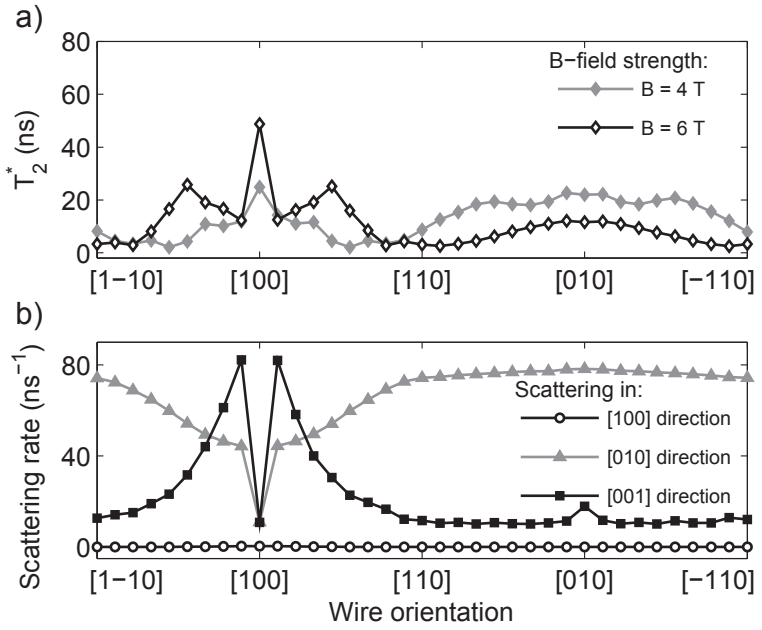

Figure 4.7: Spin dephasing time and momentum scattering rates in wires in an external magnetic field along [100]. (a) The spin dephasing time T_2^* for different wire orientations at 4 Tesla and 6 Tesla. (b) The momentum scattering rate for motion in specific directions at B=4 Tesla. The scattering rate represents the amount of scattering for motion in both (positive and negative) directions in the specified direction.)

We now discuss the features visible in Figure 4.7, with T_2^* plotted versus wire orientation, for external fields of 4 and 6 Tesla in the [100] direction. Even though the magnetic fields felt by the spins are now larger, cyclotron orbits (with a radius small compared to the wire width) appear to greatly preserve the spin states of the electrons (T_2^* of tens of nanoseconds, compared to under a nanosecond previously). This can be attributed to the fact that electrons at equal angles to the external field will have the same cyclotron orbits, and therefore experience no dephasing with respect to each other. This increased uniform behaviour is mostly hindered in our model by scattering events in the wire. Therefore, to explain different dephasing for different wire orientations, we will make a direct connection to scattering rates on the sides of the wire, for these different orientations. We will discuss several cases, where the wire is oriented in different directions with respect to the applied external field.

Firstly, when the wire is almost aligned with the external field, the particles reach the sides of the wire less frequently because of their cyclotron orbits along the external field, visible as a dip in the scattering in the [010] direction between wire orientations of [1-10] and

[110] in Figure 4.7b. Because of this dip in scattering, more cyclotron orbits are completed uninterrupted, and the dephasing time goes up.

When the wire becomes more fully aligned with the field, however, there appears a large rise in scattering in the [001] direction, visible in Figure 4.7b. This is due to particles hitting the sides of the wire, and not being able to move away from the side anymore: they form skipping orbits, skipping along the side, along the top and bottom of the wire. This happens to particles with progressively small cyclotron orbits, the smaller the angle between field and wire becomes. These orbits, which are not traversed fully, are detrimental to the dephasing time, and so when more and more particles enter skipping orbits, the dephasing time goes down. When the wire and field are exactly aligned, however, no particles reach the sides anymore, and scattering in all directions drops down significantly, causing the most major peak in spin lifetimes.

When the wire becomes increasingly oriented perpendicular to the field (towards the [010] direction), it can be seen that dephasing times rise somewhat again, an effect that goes down for increasing magnetic field. This can be attributed to the motional-narrowing effect dominant in 2D populations, where the electrons scatter back and forth against the sides of the wire, inverting and so undoing the precession with each scattering. And indeed, this effect should become less pronounced as the field strength increases, and thereby the spin precession length decreases.

Looking at the symmetries between Figures 4.7a and 4.7b, the several features of the SDA in a bulk sample in a large magnetic field can be explained. No signs remain of the symmetries in the SO-terms contributing to the SDA profile. However, these results should be taken with a grain of salt: in a real experiment, the bulk population spin lifetimes are limited by electron-hole recombination, which has its own lifetime of under a nanosecond [22]. Therefore this final part of the study is mostly useful in showing the relative importance of the different magnetic fields, and not as a prediction of a real experiment.

4.4 Conclusions

A numerical tool was presented for studying the temporal evolution of spin ensembles in micronscale structures of bulk GaAs material. Our modeling tool is based on a semiclassical picture for the electron spin in the material. Simulations with this tool show SDA for electron ensembles in quasi-ballistic wires. These calculations serve as a theoretical background for effects which have been observed experimentally. The spin dephasing times and SDA for material parameters were defined as in previous experiments in our group, and find reasonable agreement.

By comparing results for specular and non-specular momentum scattering on the edges of the wires it was found that the spin dephasing anisotropy in three-dimensional wires with specular scattering arises due to a different mechanism than confinement-enhanced motional narrowing. The observed SDA is attributable to a new mechanism that can be pictured as ballistic spin resonances that occur due to the interplay between repetitive scattering trajectories and the symmetries in the spin-orbit fields. Notably, this already occurs when the spin precession length is smaller than the transverse wire dimensions. These SDA findings agree with the experimental results (for which specular scattering is indeed expected), while the motional narrowing picture does not. Analysis which tried to identify responsible symmetries in repetitive particle trajectories did not succeed. Spin orientation with respect to the fields,

and weighting of different trajectories were not yet included in this investigation, since doing so would make the math extremely ungainly, but further insight might be gained from that approach.

Also the effect of an external magnetic field on a spin polarized bulk electron ensemble in a wire was investigated. For values of the magnetic field where the cyclotron radius is smaller than the wire width, the external field dominates the SDA, instead of the SO-field symmetry. These results are very sensitive to the alignment of the wire with respect to the magnetic field and the crystallographic axes. However, since the predicted times are way in excess of realistic electron-hole recombination times in a bulk material, and the spin population there consists entirely of excited fre electrons, these results are not indicative of the outcome of a real experiment. Rather, they illustrate the relative importance of the SO-fields and external magnetic fields. However, the disappearance of the SDA, present in bulk material without an external field, finds correspondence with previous experiments.

We thank S. Artyukhin and A. Rudavskyi for help and valuable discussions and acknowledge the support of the High Performance Computing Center at the University of Groningen.

Bibliography

[1] M. I. D'yakonov and V. I. Perel, Sov. Phys. Solid State **13**, 3023 (1972).

[2] R. H. Silsbee, J. Phys. Condens. Matter **16**, R179 (2004).

[3] G. Dresselhaus, Phys. Rev. **100**, 580 (1955).

[4] N. S. Averkiev, L. E. Golub, and M. Willander, J. Phys.: Condens. Matter **14** R271 (2002).

[5] R. Winkler, *Spin-Orbit Coupling Effects in Two-Dimensional Electron and Hole Systems*, Springer Tracts in Modern Physics Vol. 191 (Springer, Berlin, 2003).

[6] B. Andrei Bernevig, J. Orenstein, and Shou-Cheng Zhang, Phys. Rev. Lett. **97**, 236601 (2006).

[7] M. Duckheim and D. Loss, Phys. Rev. B **75**, 201305(R) (2007).

[8] M. Duckheim, D. L. Maslov, and D. Loss, Phys. Rev. B **80**, 235327 (2009).

[9] M. Duckheim, D. Loss, I. Adagideli, and P. Jacquod, Phys. Rev. B **81**, 085303 (2010).

[10] J. D. Koralek, C. P. Weber, J. Orenstein, B. A. Bernevig, Shou-Cheng Zhang, S. Mack, and D. D. Awschalom, Nature (London) **458**, 610 (2009).

[11] A. W. Holleitner, V. Sih, R. C. Myers, A. C. Gossard, and D. D. Awschalom, Phys. Rev. Lett. **97**, 036805 (2006).

[12] S. Z. Denega, T. Last, J. Liu, A. Slachter, P. J. Rizo, P. H. M. van Loosdrecht, B. J. van Wees, D. Reuter, A. D. Wieck, C. H. van der Wal, Phys. Rev. B **81**, 153302 (2010).

[13] J. Fabian, A. Matos-Abiague, C. Ertler, P. Stano, and I. Zutic, *Semiconductor Spintronics*, Acta Phys. Slov. **57**, 565 (2007).

[14] J. Liu, T. Last, E. J. Koop, S. Denega, B. J. van Wees, C. H. van der Wal, J. Supercond. Nov. Magn. **23**, 11 (2010).

[15] S. Lüscher, S. M. Frolov, J. A. Folk, Phys. Rev. B **82**, 115304 (2010).

[16] M. Studer, G. Salis, K. Ensslin, D.C. Driscoll, and A.C. Gossard, Phys. Rev. Lett. **103**, 027201 (2009).

[17] J. H. Bardarson, Diss., Universiteit Leiden, Leiden, print (2008).

[18] J. M. Kikkawa and D. D. Awschalom, Phys. Rev. Lett. **80**, 4313 (1998).

[19] S. Z. Denega, Diss., Rijksuniversiteit Groningen, Groningen, print (2011).

[20] E. J. Koop, B. J. van Wees, C. H. van der Wal, arXiv:0804.2968 (2008).

[21] Z. H. Sainz, BSc. thesis, Rijksuniversiteit Groningen, Groningen, print (2010).

[22] E. J. Koop, Diss., Rijksuniversiteit Groningen, Groningen, print (2008).

[23] W. W. Yu, S. M. Frolov, S. Lüscher, J. A. Folk and W. Wegscheider, arXiv:1009.5702 (2010).

[24] S. M. Frolov, S. Lüscher, W. Yu, Y. Ren, J. A. Folk, and W. Wegscheider, Nature (London) **458**, 868 (2009).

Acknowledgements

Rounding up a year of research, I think it would be fitting to extend thanks to the people who helped me through it.

First and foremost, I am indebted to my direct supervisor Sergii Denega, who has always been available for advise, discussion, oranges and cherry-flavoured yoghurt (of which he ows me a few packs, when he finds a new job - you know what I'm talking about Sergii). We've shared some frustrations and we've shared some revalations, and I thank you for everything.

Also to my super-supervisor Caspar van der Wal, many thanks not only for effectively guiding the project along and being so cheerfull all the time, but also thanks for helping me get to where I am typing this right now: MIT in Boston, Massachusetts, where I'll be doing an internship for some 6 months. Weirdly enough there are breakdancers in the never-locked entry hall of my lab here, apparently almost every day from 5PM on, but I suppose they don't interfere with world-class research.

Also my thanks go out to Muhammad Javaid Iqbal, who stuck by me when pouring dangerous fluids together in the cleanroom, and got enormously enthusiastic when explaining the finer points of cricket. I explained it to some others since then, without them pointing out logical impossibilities, so I think I got it.

I could go on like this, since nearly every PhD or PostDoc in FND has been called into action on my behalf at some point during my research, but that would grow tiring, so: thank you all very much. The atmosphere was great, and I hope your devices will be kind to you.

Stepping outside of FND, I'd like to thank my parents for unwavering support, even when I came home to them, ranting about etching that didn't work. I remember playing a childish joke on my father by writing in my bachelor's thesis: "I'd also like to thank my father, without whom this research would have turned out exactly the same". I'd like to take that back now.

Finally, I'd like to thank the one that has over the past 20 months become the light of my life, my wonderful girlfriend Laura.

Appendix A

Device fabrication steps

1) Device etching

• Preparation:
- Cut wafer with resist on top (to prevent cutting particle contamination)
- Clean in two beakers of boiling acetone (10" and 20')
- Clean in ultrasonic bath in warm acetone on teflon holder (10', power 2)
- Spin dry
- Bake 30'
- Oxygen plasma cleaning (80", power 40 W, flow 9 sccm, pressure 0.016 mBar)

• Resist:
- Spin 70 nm 950K PMMA (2% in Ethyl lactate) - 4000 rpm (60")
- Bake at 180 °C (2h)

• First exposure (large structures and wire alignment markers):
- Beam voltage: 10 keV
- Aperture: 60 μm
- Working area: 2000 x 2000 μm
- E-beam dose: 260 μC/cm^2

• Developing:
- Develop in 1:3 MIBK / IPA (35")
- Rinse in IPA (30")
- Spin dry
- Bake at 180 °C (30')

• Second exposure (wires):
- Beam voltage: 10keV
- Aperture: 10 μm
- Working area: 300 x 300 μm
- E-beam dose: 260 μC/cm^2

• Developing:

- Develop in 1:3 MIBK / IPA (35")
- Rinse in IPA (30")
- Spin dry
- Bake at 180 °C (30')

• Etching:
- Etch in a 1:1:50 solution of H_2SO_4 / H_2O_2 / H_2O (50", etch rate approximately 2 nm/s)
- Rinse in three beakers of H_2O (10", 60", 60")
- Spin dry

• Cleaning:
- Clean in boiling acetone (10')
- Rinse in IPA (30")
- Spin dry

2) Ohmic contacts:
• Preparation
- Clean in boiling aceton (10")
- Rinse in IPA (30")
- Spin dry

• Resist:
- Spin 400 nm 50K PMMA (9% in Chlorobenzene) - 4000 rpm (60")
- Bake at 180 ^{circ}C (15')
- Spin 70 nm 950K PMMA (2% in Ethyl lactate) - 4000 rpm (60")
- Bake at 180 ^{circ}C (15')

• Exposure:
- Beam voltage: 10 keV
- Aperture: 120 μm
- Working area: 2000 x 2000 μm
- E-beam dose: 200 μC/cm^2

• Developing:
- Develop in 1:3 MIBK / IPA (60")
- Rinse in IPA (30")
- Spin dry

• Evaporation:
- 1 nm Ti (optional, for better adhesion of the metal to the wafer)
- 120 nm AuGe
- 30 nm Ni
- 20 nm Au

• Lift-off:
- Lift-off in acetone (several hours) / acetone spray

- Rinse in IPA (30")
- Spin dry

• Annealing:
- Anneal in N^2 atmosphere (50 ml/s) in the oven at 450 ^{circ}C (5')

3) Bond pads:
• Preparation:
- Clean in boiling aceton (10")
- Rinse in IPA (30")
- Spin dry

• Resist:
- Spin 250 nm 950K PMMA (4% in Chlorobenzene) - 4000 rpm (60")
- Bake at 180 ^{circ}C (15')

• Exposure:
- Beam voltage: 10 keV
- Aperture: 60 μm
- Working area: 2000 x 2000 μm
- E-beam dose: 100 $\mu C/cm^2$

• Developing:
- Develop in 1:3 MIBK / IPA (35")
- Rinse in IPA (30")
- Spin dry

• Evaporation:
- 5 nm Ti
- 50 nm Au

• Lift-off
- Lift-off in acetone (several hours) / acetone spray
- Rinse in IPA (30")
- Spin dry

4) Transparant gates:
• Preparation:
- Clean in boiling aceton (10")
- Rinse in IPA (30")
- Spin dry

• Resist:
- Spin 370 nm 950K PMMA (4% in Ethyl lactate) - 3000 rpm (60")
- Bake at 180 ^{circ}C (15')

- Spin 250 nm 950K PMMA (4% in Ethyl lactate) - 4000 rpm (60")
- Bake at 180 ^{circ}C (15')

• Exposure:
- Beam voltage: 10 keV
- Aperture: 60 μm
- Working area: 2000 x 2000 μm
- E-beam dose: 140 μC/cm^2

• Developing:
- Develop in 1:3 MIBK / IPA (35")
- Rinse in IPA (30")
- Spin dry

• RF sputtering SiO_2:
- 300 nm SiO_2 (2h)

• Lift-off:
- Lift-off in ultrasonic bath in warm acetone on teflon holder (10', power 2)
- Rinse in IPA (30")
- Spin dry

• Resist:
- Spin 370 nm 950K PMMA (4% in Ethyl lactate) - 3000 rpm (60")
- Bake at 180 ^{circ}C (15')
- Spin 250 nm 950K PMMA (4% in Ethyl lactate) - 4000 rpm (60")
- Bake at 180 ^{circ}C (15')

• Exposure:
- Beam voltage: 10 keV
- Aperture: 60 μm
- Working area: 2000 x 2000 μm
- E-beam dose: 140 μC/cm^2

• Developing:
- Develop in 1:3 MIBK / IPA (35")
- Rinse in IPA (30")
- Spin dry

• DC sputtering ITO:
- 150 nm ITO (25')

• Lift-off:
- Lift-off in ultrasonic bath in warm acetone on teflon holder (10', power 2)
- Rinse in IPA (30")
- Spin dry

Appendix B

Matlab simulation code

The following pages contain the base form of the code used to run the simulations, presented in chapter 4, except for the programs sinrand.m and keep.m. All code is also included on a cd, which should be present at the back of this thesis (if not, and you want one: contact Caspar van der Wal, at the email adress listed in an annotation in the masterprogram). Since the numerical experiment gets its results from averaging over many randomly initialized iterations of the same experiment, it falls in the category of Monte Carlo simulations. The program essentially does the following, which will also be the sequence in which the programs will be presented:

"masterprogram3D.m"

iterates for different wire orientations, calling on

"spinorbwire.m"

which generates random starting positions and momenta for 1000 particles, that will move around in a box for a certain simulation time, governed by the physical parameters and constants listed in

"parameters.m"

Spinorbwire.m also calls on the function

"differentials.m"

to determine the actual trajectory for each particle between collisions. This function that allows a differential equation solver from matlab to calculate the trajectory, based on the force balance, which consists solely of the lorentz force, and the momentum initial values. Some other programs are used ("parameters.m", containing the physical constants and wire dimensions, "sinrand.m", allowing for proper random distribution on a sphere, "keep.m", allowing for efficient removal of all arrays except for the ones you want to keep). These simulations are so computationally intensive that they need to be parallellized, and if run on the Millipede network of the RuG with the PBS file masterprogram3D.PBS, many of

these eight-core simulations can be run at the same time, cutting back on computation time enormously. Due to time restraints on this network, several iterations of the masterprogram need to be run for fewer particles than are eventually necessary, and should eventually be added. Information of how to run parallel matlab code on this network can be found here: http://www.rug.nl/cit/hpcv/publications/docs/millipede. To prevent files being overwritten when running the same identical simulation several times, saving the same filenames to the same folder, the time of saving is added to the filename. Files from these simulations must therefore undergo name changing to remove the timestamp in the filename, and have "_1", "_2" or higher appended before the extension, depending how many iterations of the code were done, which can be done with many programs. Then, they can then be post-processed by the program

"particleadder.m"

which adds the results of identical iterations of the program. These results can then be processed by

"readout.m"

which generates arrays with decay traces of $< S_r >$ versus time, for the different orientations of the wire, after which the combination of

"T2stars.m" and "fitexp.m"

can extract the T_2^* values for the different orientations. This is the data that has been presented in chapter 4, for several experimental variables. Many more is explained in extensive comments, inside the code.

Masterprogram3D.m:

```
% This program will save spin ensemble data for some set amount of
% particles, defined in the parameters.n file. Running on the Millipede
% network, on 8 cores, it can produce one file containing data for 250
% particles every 2h 15' or so (varies depending on the amount of
% scattering particles randomly have).

% The maximum walltime is 175h, so this is your limiting factor. If this
% program is run 4 times in parallel for 250 particles per program, you
% end up with data for 1000 particles, a good amount for statistics. A
% single run of the program, for all the angles for one specific field
% strength, then takes around 5 days.

% Then, the data from the four files should be merged, by loading the
% seperate average spin arrays, adding them, and dividing by how many files
% are used, to get the proper spin averages.

% To be able to run these 4 simulations at the same time, I use a timestamp
% in the save file name, so that two files for the same angle, field, and
% in the same folder won't overwrite each other. To merge the files, a good
% way is to remove this timestamp, and label the 4 files 1 through 4. Then,
% a small matlab program can add the files together (added in the appendix
% as "particleadder.m"). The actual filename changing I did with the GUI
% "R-name", a Mac application, since it seemed too complicated to have
% matlab find the proper files and rename them, but it would be a nice
% addition to have matlab do this as well in the future. The resulting data
% can be read out with the program "readout.m", giving as output an array
% of <Sr> versus time traces, for 37 different angles (-45 to +135 degrees
% with respect to the [100] axis), named "spinravesBis#", and number of
% scatterings for positive and negative x,y and z faces of the wire, during
% the entire simulation. Finally, T2stars.m will take these traces, and
% through fitting of exponents extract the value for T2* for every
% orientation of the wire.




%For generation of a true random stream. This stream also supports
%substreams for the different parfor loops (important, else all you parfor
%loops wil be identical):
stream = RandStream('mlfg6331_64','Seed',sum(100*clock));

%This defines how many cores are used for he parallel computation. The
%maximum number matlab can currently handle is 8, but this is supposed to
```

```
%be increased in future editions. The RuG computer cluster Millipede has
%nodes with, at least, 12 cores, so some will be idle when used like
%this...
matlabpool(8);

%Here the external magnetic fields are defined. It is also possible to pass
%these to the program using the PBS-script, but since they need to be
%written down somewhere anyway (you can't pass a function argument to
%millipede), it might as well be here.

%%%%%%%%%%%%%%%%%%%%%%%%%%%%%%%%%%%%%%%%%%%%
                  Bx=0;
                  By=0;
                  Bz=0;
%%%%%%%%%%%%%%%%%%%%%%%%%%%%%%%%%%%%%%%%%%%%

Bext=[Bx By Bz];

%The try-catch structure ensures that, if simething goes wrong during the
%simulation (and the Millipede network sometimes does unexpected nonsense),
%the matlabpool is closed.
try

for alpha = -45:5:135 %in degrees

        alpha = alpha*pi/180; %in radians
        spinorbwire;
        % what will be saved:
        keep alpha Bext time spinXAve spinYAve spinZAve spinThetaAve...
             spinPhiAve spinRAve stream Xplus Xminus Yplus Yminus Zplus...
             Zminus;
        % the path should be changed if the program is run on another
        % platform. Also the account and saving folder should be changed.

        data=sprintf(...
'/data/p######/B#/3D alpha=%3.1f B=[%3.2f %3.2f %3.2f] %s parfor.mat'...
        ,(alpha/pi*180),Bext(1),Bext(2),Bext(3),datestr(now)); %for linux
        save(data);

        keep Bext stream;
end


matlabpool close
clear

catch exception
```

```
        matlabpool close
        keep exception
        save('/home/p######/error');

end
```

Spinorbwire.m:

```
% Spin-orbit simulator in QUASI-1D quantum wire systems.

% Original version authors/users:
% Ji Liu - j.liu@rug.nl (not in use anymore)
% Caspar van der Wal - c.h.van.der.wal@rug.nl
% Erik Koop - e.j.koop@rug.nl (not in use anymore)

% This version by:
% Olger Zwier - olgerzwier@gmail.com

% Version of 20 June 2011.

% Features:
%   3D motion, with Lorentz force induced spiraling electron motion.
%   Can be switched between specular and non-specular scattering.
%   Easily tweaked to solve for any other variation of parameter from the
%   masterprogram.
%   New parfor version that should be run on RuG Millipede network
%   (because of computational intensity).
%   Includes transform for Q1D wire in arbitrary direction.

% Program assumes the convention that the +z-direction is the
% [001] crystal orientation, and the growth direction for the 2D and 1D
% materials.
```

```
%%%%%%%%%%%%
% PREAMBLE %
%%%%%%%%%%%%
```

```
% To load the physical constants wire dimensions

%%%%%%%%%%%%%%%%
parameters;
%%%%%%%%%%%%%%%%
```

```
% Forward coordinate transform to new XY coordinates in wire reference
% from crystal frame:

CoTrF11 =  cos(alpha);
CoTrF12 =  sin(alpha);
CoTrF21 = -sin(alpha);
CoTrF22 =  cos(alpha);

% Backward coordinate transform to from XY coordinates in wire reference
% back to crystal frame:

CoTrB11 =  cos(alpha);
CoTrB12 = -sin(alpha);
CoTrB21 =  sin(alpha);
CoTrB22 =  cos(alpha);
```

```
% Check if the time step is small enough to resolve the physical effects:
spacestep = vFmag*dt;

reldotsizestep = min([L,W])/spacestep;
if reldotsizestep < 2
   display('##### WARNING, time step too large for dot size! #####');
end

relscatterstep = scattertime/dt;
if relscatterstep < 2
   display('##### WARNING, time step too large for scattertime! #####');
end
```

```
% Pre-allocate here the 5 initial momentum and spin arrays
% that are not updated further in the parfor program

kxstart = zeros(numspin,1);
kystart = zeros(numspin,1);
kzstart = zeros(numspin,1);
thetastart = zeros(numspin,1);
phistart = zeros(numspin,1);

% Initialize here the momentum arrays. ktheta is NOT pi*rand(1), since
% such a distribution would make the majority of particles go in the +- z
% directions: each circle at each height along z would have equally many
% points, while the radius of the circles decreases with height. A sine
% like weighting function is therefore needed, defined in sinrand.m.

for spinpart = 1:numspin
   kphi=2*pi*rand(1);
   ktheta=sinrand;
   kxstart(spinpart)        = kFmag*cos(kphi)*sin(ktheta);
   kystart(spinpart)        = kFmag*sin(kphi)*sin(ktheta);
   kzstart(spinpart)        = kFmag*cos(ktheta);
end
```

```
%%%%%%%%%%%%%%%%%%%%%%
% LOOP OVER PARTICLES %
%%%%%%%%%%%%%%%%%%%%%%
```

```
% Since the program now runs the timeloop inside the particle loop again
% bacause of the parfor structure, it is not possible to have it stop when
% the average spin drops beneath some limit, so the while loop is replaced
% by a for. Reasonable boundaries then need to be set in the parameters.m
% file, such as 1 or 10 nanoseconds as total run time for 1000 particles.

parfor spinpart = 1:numspin

       set(stream,'Substream',spinpart); %so that not every parfor
                                         %iteration uses the same random
```

```
                                        %numbers
   prevstream = RandStream.setDefaultStream(stream); %this actually
                                                     %makes it the
                                                     %used stream

% These counters will store how many times every particle bounces from
% an edge.

   XXplus=0;
   XXminus=0;
   YYplus=0;
   YYminus=0;
   ZZplus=0;
   ZZminus=0;

% Here we pre-allocate the spin vectors (labeled with extra capital)
% to be used within parfor, eventually to be stored as part of its
% respective spin matrix outside of the for loop.

    spinXX          = zeros(1,timesteps);
    spinYY          = zeros(1,timesteps);
    spinZZ          = zeros(1,timesteps);
    spinThetaTheta  = zeros(1,timesteps);
    spinPhiPhi      = zeros(1,timesteps);

% Initialize the starting positions and define the momenta (different
% for every parfor loop, because of the different substreams from the
% random stream for eacht iteration of the loop!). The momenta are
% initialized outside of parfor to avoid problems with the "sinrand"
% function.

    XW        = L*rand(1)-L/2;
    YW        = W*rand(1)-W/2;
    ZW        = H*rand(1)-H/2;

    X         = CoTrB11*XW    +   CoTrB12*YW;
    Y         = CoTrB21*XW    +   CoTrB22*YW;
    Z         = ZW;

    kx        = kxstart(spinpart);
    ky        = kystart(spinpart);
    kz        = kzstart(spinpart);

    IniSpinState = [1 0];
    theta        = 2*acos(real(IniSpinState(1)));
    phi          = angle(IniSpinState(2));
```

```
  Rot=zeros(2,2); % pre-allocated, so the parfor can handle it.
  Bdress3=zeros(1,3); % the same as above.




                        %%%%%%%%%%%%%%%%%
                        % LOOP OVER TIME %
                        %%%%%%%%%%%%%%%%%


for timeindex=1:timesteps

     % starting conditions for the ode solver:
        vX=hbar*kx/mEff;
        vY=hbar*ky/mEff;
        vZ=hbar*kz/mEff;

     % the function differentials.m contains the general form of the
     % Lorentz force equation of motion, and is solved with a
     % Runge Kutta solver pre-made in matlab (the 4-5 one with
     % medium accuracy, which has been checked to perfecly follow
     % the cyclotron orbits). First though, we define "tosolve" as
     % the differential equation function that has had the external
     % field passed inside, since the ode45 solver does not want the
     % external fields passed as arguments to it directly:

        tosolve = @(t,v) differentials(t,v,Bext(1),Bext(2),Bext(3));
        [t,v] = ode45(tosolve,[0,dt],[vX;vY;vZ]);

        % the k-vector in the crystal frame will continue to be used
        % for the spin precession steps. The index of the velocity
        % vectors will also be the index for this k-vector, and as
        % soon as the particle trajectory is changed because of
        % scattering, the k-vector is updated along with it.
        % Essentially, the particle movement happens in the wire
        % frame, and in parallel, the spin precession is done in the
        % crystal frame (necessary, since the SO-fields are defined
        % along those axes).

        k = mEff*v/hbar;

      % for being able to take a period of time from vector t around
      % the velocity at that index, t is padded with an extracted
```

```
% value at the start and the end (so that the loop can take a
% (t(n+1)-t(n-1))/2 value at the first and final nodes). From
% here on the indices of t are therefore shifted (n=5
% corresponds to the node n=4 in v and k):

  t=transpose(t);
  t=[t(1)-(t(2)-t(1)) t];
  t=[t t(length(t))+(t(length(t))-t(length(t)-1))];

% v in the wire frame, the vectors used for actual particle
% movement:

  vXW   = CoTrF11*v(:,1)   + CoTrF12*v(:,2);
  vYW   = CoTrF21*v(:,1)   + CoTrF22*v(:,2);
  vZW   = v(:,3);

  dtremain = dt; % the time that remains of dt (at m=1, equal
                 % to dt)

  m=1; % m counts the steps of the ode solver within one dt
       % time step


while m<length(t)-1

    dtprecess = dtremain;

    while abs(XW)<L2 && abs(YW)<W2...
       && abs(ZW)<H2 && m<length(t)-1

        % single steps in x,y and z:
        XW = XW + vXW(m)*(t(m+2)-t(m))/2;
        YW = YW + vYW(m)*(t(m+2)-t(m))/2;
        ZW = ZW + vZW(m)*(t(m+2)-t(m))/2;
```

```
%%%%%%%%%%%%%%%%%%
% SPIN PRECESSION %
%%%%%%%%%%%%%%%%%%
```

```
   % The spin precession steps are also explicitly
   % written out because they need to be, according to
   % the parfor demand for "transparancy". The
   % precession is carried out each time the particle
   % does not reach a boundary after a very small step
   % along its path, as resolved by the above
   % differential equation.

   Bdress1 = Cdress1*[ -k(m,1) k(m,2) 0];

   Bdress3(1,1) = Cdress3*k(m,1)*(k(m,2)^2-k(m,3)^2);
   Bdress3(1,2) = Cdress3*k(m,2)*(k(m,3)^2-k(m,1)^2);
   Bdress3(1,3) = Cdress3*k(m,3)*(k(m,1)^2-k(m,2)^2);

   Brashba = Crashba*[ k(m,2) -k(m,1) 0];

   Btot = Bext + Bdress1 + Bdress3 + Brashba;
   Bmag = norm(Btot);

   if Bmag == 0 % To avoid devision by zero for B = 0.
      Bmag = 1;
   end

   PrecessAngle = -gUb*Bmag*(t(m+2)-t(m))/2/hbar;
   % The minus sign is because (given gUb)
   % the electron spin precesses in a left-handed sense
   % around the vector B for gUb>0.
   % See notes Caspar and Ji of 2 September 2005.
   p2 = PrecessAngle/2; %abbreviaton

   % Unit vector the spin precesses around:
   ux = Btot(1)/Bmag;
   uy = Btot(2)/Bmag;
   uz = Btot(3)/Bmag;

   % The rotation operator on the spin state.
   % See the book "Quantum Mechnanics"
   % by Cohen-Tannoudji, p.699 and p. 985.
   Rot(1,1) = cos(p2) - 1i*uz*sin(p2);
   Rot(1,2) = -(1i*ux + uy)*sin(p2);
   Rot(2,1) = -(1i*ux - uy)*sin(p2);
   Rot(2,2) = cos(p2) + 1i*uz*sin(p2);

   % Program still knows theta and phi from (time-1).
OldSpinstate = [cos(theta/2);sin(theta/2)*exp(1i*phi)];

   NewSpinstate = Rot*OldSpinstate;
```

```
        % Remove an arbitrary global phase in the state.
        GlobPhase = angle( NewSpinstate(1) );
        NewSpinState = NewSpinstate*exp(-1i*GlobPhase);

        % Calculate new theta and phi for this round (time).
        theta = 2*acos(real( NewSpinState(1) ));
        phi   = angle( NewSpinState(2) );




m=m+1;
end




    %%%%%%%%%%%%%%%%%%%%%%
    % SPECULAR SCATTERING %
    %%%%%%%%%%%%%%%%%%%%%%


m=m-1; % 15 lines back, the simulation moved on to the
       % next step, but if the particle scattered, we want
       % the index m for which it did, so we go back one
       % step again.

   % The following checks, along the path from ODE45, from
   % which wall(-s) the particle scatters after a minimal
   % step. Also: let the particle take one mniscule step
   % back into the box (to avoid calculation difficulties
   % where the particle is outside the box, and the next
   % step does not take it into the box again: Then a
   % particle can weirdly stay outside of the box and
   % cause the program to return crashes and errors). The
   % part commented after is a variation on this
   % scattering code, that will make the particles scatter
   % non-specularly, instead of specularly.

   %%{
   if abs(XW)>=L2
        dtprecess = (t(m)+t(m+1))/2;
        XW = XW-vXW(m)*(t(m+2)-t(m))/2;
```

```
        vXW(m) = -vXW(m);
        vYW(m) = vYW(m);
        vZW(m) = vZW(m);
        if sign(XW)==1
            XXplus=XXplus+1;
        else
            XXminus=XXminus+1;
        end
    end
    if abs(YW)>=W2
        dtprecess = (t(m)+t(m+1))/2;
        YW = YW-vYW(m)*(t(m+2)-t(m))/2;
        vXW(m) = vXW(m);
        vYW(m) = -vYW(m);
        vZW(m) = vZW(m);
        if sign(YW)==1
            YYplus=YYplus+1;
        else
            YYminus=YYminus+1;
        end
    end
    if abs(ZW)>=H2
        dtprecess = (t(m)+t(m+1))/2;
        ZW = ZW-vZW(m)*(t(m+2)-t(m))/2;
        vXW(m) = vXW(m);
        vYW(m) = vYW(m);
        vZW(m) = -vZW(m);
        if sign(ZW)==1
            ZZplus=ZZplus+1;
        else
            ZZminus=ZZminus+1;
        end
    end
    %}
```

```
%%%%%%%%%%%%%%%%%%%%%%%%%%%%%%%%%%%%
% NON-SPECULAR SCATTERING
%%%%%%%%%%%%%%%%%%%%%%%%%%%%%%%%%%%%
```

```
%{

% The values vYW(m) and vZW(m) are stored, to prevent
% the program from randomizing vYW(m) and vZW(m), and
% then taking the "step back into the box", with a step
% that might not anymore lead into the box at all!

vYstor = vYW(m);
vZstor = vZW(m);

if abs(XW)>=L2
     dtprecess = (t(m)+t(m+1))/2;
     XW = XW-vXW(m)*(t(m+2)-t(m))/2;
     vPhi = pi*rand(1)+sign(XW)*pi/2;
     vtheta = sinrand();
     vXW(m) = vFmag*cos(vPhi)*sin(vtheta);
     vYW(m) = vFmag*sin(vPhi)*sin(vtheta);
     vZW(m) = vFmag*cos(vtheta);
     if sign(XW)==1
         XXplus=XXplus+1;
     else
         XXminus=XXminus+1;
     end
end
if abs(YW)>=W2
     dtprecess = (t(m)+t(m+1))/2;
     YW = YW-vYstor*(t(m+2)-t(m))/2;
     vPhi = pi*rand(1)+(sign(YW)+1)*pi/2;
     vtheta = sinrand();
     vXW(m) = vFmag*cos(vPhi)*sin(vtheta);
     vYW(m) = vFmag*sin(vPhi)*sin(vtheta);
     vZW(m) = vFmag*cos(vtheta);
     if sign(YW)==1
         YYplus=YYplus+1;
     else
         YYminus=YYminus+1;
     end
end
if abs(ZW)>=H2
     dtprecess = (t(m)+t(m+1))/2;
     ZW = ZW-vZstor*(t(m+2)-t(m))/2;
     vPhi = 2*pi*rand(1);
     if sign(ZW) == 1
         vtheta = sinrand2();
     else
         vtheta = sinrand3();
     end
```

```
            vXW(m) = vFmag*cos(vPhi)*sin(vtheta);
            vYW(m) = vFmag*sin(vPhi)*sin(vtheta);
            vZW(m) = vFmag*cos(vtheta);
            if sign(ZW)==1
                ZZplus=ZZplus+1;
            else
                ZZminus=ZZminus+1;
            end
        end
        %}

        dtremain = dtremain-dtprecess; % time left of dt
                                       % (=0 if no boundary
                                       % was encountered and
                                       % dtremain = dtprecess!)

        if dtremain > 0
        % The coordinates are taken back to their crystal frame
        % values, because the motion differential equation is
        % solved in that coordinate frame, and the magnetic
        % field is defined there.

       vX   = CoTrB11*vXW(m)   + CoTrB12*vYW(m);
       vY   = CoTrB21*vXW(m)   + CoTrB22*vYW(m);
       vZ   = vZW(m);

       t=0; % these values are NOT "unused": they serve to
       v=0; % eliminate the highest indexed elements from the
       k=0; % previous solution to the ode45, so that they
            % do not show up in the next solution for t,v and k
            % (since the ode45 solver does not give a fixed
            % length for the number of steps it takes to solve
            % an equation).

   tosolve = @(t,v) differentials(t,v,Bext(1),Bext(2),Bext(3));
       [t,v] = ode45(tosolve,[0,dtremain],[vX;vY;vZ]);
       k = mEff*v/hbar;

       t=transpose(t);
       t=[t(1)-(t(2)-t(1)) t];
       t=[t t(length(t))+(t(length(t))-t(length(t)-1))];

       vXW   = CoTrF11*v(:,1)   + CoTrF12*v(:,2);
       vYW   = CoTrF21*v(:,1)   + CoTrF22*v(:,2);
       vZW   = v(:,3);

       m=1;
```

```
            elseif dtremain == 0
              t=0; % t and v (and later k) must be reset to zero, so
                   % that their last entries won't show up in future,
              v=0; % possibly shorter t,v and k arrays
            elseif dtremain < 0
              display('DANGER WILL ROBINSON!!!');
            end
      end
```

```
%%%%%%%%%%%%%%%%%%%%%%%%%%%%%%%%%%%%%%
% MOMENTUM SCATTERING (EXPONENTIAL) %
%%%%%%%%%%%%%%%%%%%%%%%%%%%%%%%%%%%%%%
```

```
% Here after one step dt the particle may or may not momentum
% scatter:

Unirannum = rand(1);

if Unirannum > Pnot
  kPhi = 2*pi*rand(1);    %% after scattering k vector of electron
  ktheta = sinrand;       %% is randomly oriented
  kx   = kFmag*cos(kPhi)*sin(ktheta);
  ky   = kFmag*sin(kPhi)*sin(ktheta);
  kz   = kFmag*cos(ktheta);
else
  kx = k(length(k),1);
  ky = k(length(k),2);
  kz = k(length(k),3);
end

% For the same reason t and v were reset to zero:
k=0;


 % This fills up the spin array for a single particle in its parfor
 % loop (one entry every timestep in for):

 spinXX(timeindex) = sin(theta)*cos(phi);
```

```
        spinYY(timeindex) = sin(theta)*sin(phi);
        spinZZ(timeindex) = cos(theta);
        spinThetaTheta(timeindex) = theta/pi; % In units of pi!
        spinPhiPhi(timeindex) = phi/pi;  % In units of pi!



        end %end of for loop over time

        %Here the spin matrices are filled with the parallel running arrays
        %for each spinpart:

        spinX(spinpart,:) = spinXX;
        spinY(spinpart,:) = spinYY;
        spinZ(spinpart,:) = spinZZ;
        spinTheta(spinpart,:) = spinThetaTheta;
        spinPhi(spinpart,:) = spinPhiPhi;

        %Here the edge-collision counters for each spinpart are filled:

        Xplus(spinpart) = XXplus;
        Xminus(spinpart) = XXminus;
        Yplus(spinpart) = YYplus;
        Yminus(spinpart) = YYminus;
        Zplus(spinpart) = ZZplus;
        Zminus(spinpart) = ZZminus;

end %end of parfor loop over particles









                              %%%%%%%%%%%%%%%%%%
                              % POST-PROCESSING %
                              %%%%%%%%%%%%%%%%%%


for time=1:timesteps

    spinXAve(time)     = mean(spinX(:,time));
    spinYAve(time)     = mean(spinY(:,time));
    spinZAve(time)     = mean(spinZ(:,time));
    spinThetaAve(time) = mean(spinTheta(:,time)); % In units of pi!
```

```
    spinPhiAve(time)   = mean(spinPhi(:,time));   % In units of pi!
    %spinRave starts at 1 at index 1 (= time is 0), so that first spot is
    %already taken, and the calculation below starts at index 2
    spinRAve(time+1)   = sqrt( spinXAve(time).*spinXAve(time)...
                         + spinYAve(time).*spinYAve(time)...
                         + spinZAve(time).*spinZAve(time));

end
```

Parameters.m:

```
          %%%%%%%%%%%%%%%%%%%%%%%%%%%%%%%%%%%%%%%%%%%%%%%%%%
          % INITIALIZE CONSTANTS AND SIMULATION PARAMETERS %
          %%%%%%%%%%%%%%%%%%%%%%%%%%%%%%%%%%%%%%%%%%%%%%%%%%

% Some constants and parameters for the run.

dt          = 0.5*1E-12;             % Computational time step in s.

numspin     = 250;                   % Number of spins to average over.

timesteps   = 19999;                 % Number of times dt is run.

mEff        = 0.067*9.109E-31;       % Electron effective mass in GaAs in kg.

e           = 1.602E-19;             % Magnitude of the electron charge.

hbar        = 1.055E-34;             % Planck's reduced constant.

nElec       = 2.4E22;            % From "Optical probing of spin dynamics of
                                 % two-dimensional and bulk electrons in a
                                 % GaAs/AlGaAs heterojunction system",
                                 % P.J. Rizo et al, page 4, on a bulk
                                 % reference sample. From
                                 % http://arxiv.org/abs/0910.1714v1.

mobility    = 300;                   % From Andrii Rudavskyi's thesis

gUb         = (-0.44)*(-9.274E-24); % Is g*\mu_{B} for GaAs in J per Tesla.

kFmag       = (3*pi^2*nElec)^(1/3); % Magntitude of Fermi k-vector for 3D.

scattertime = mobility*(mEff/e);    % Scatter time in s.

Pnot        = exp(-dt/scattertime); % P(NOT momentum scatter after dt).

meanfreepath = (hbar*kFmag/mEff)*scattertime; % Mean free path in meters.

vFmag       = hbar*kFmag/mEff;
```

```
                        %%%%%%%%%%%%%%%%
                        % SO-PREFACTORS %
                        %%%%%%%%%%%%%%%%

% The spin-orbit parameters, with SO coupling expressed as an effective
% B-field. This requires all C<0 for GaAs, to get the signs consisitent
% with J. Miller et al., Phys. Rev. Lett. 90, 076807 (2003)!


Cdress1 = 0*-1.57E-8;      % Dresselhaus-k constant in units (Tesla meter),
                           % for 1D or 2D only.
Cdress3 = -1.17E-24;       % Dresselhaus-k^3 constant in (Tesla meter^3),
                           % for 3D only.
Crashba = 0.2967*-1.57E-8; % Rashba-k constant in (Tesla meter).




                        %%%%%%%%%%%%%%%%%%%%%%
                        % DIMENSIONS OF WIRE  %
                        %%%%%%%%%%%%%%%%%%%%%%


L            =200E-6;% Length of the box in X direction.
   L2 = L/2;
W            =1E-6;  % Width of the box in Y direction.
   W2 = W/2;
H            =1E-6;  % Width of the box in Z direction.
   H2 = H/2;
```

Differentials.m:

```
function out1 = differentials(~,v,Bx,By,Bz)

% v in vector notation:
    v = [v(1) v(2) v(3)];

% the constants used for the Lorentz force balance:
    mEff = 0.067*9.109E-31;        % Electron effective mass in GaAs in kg.
    e = 1.602E-19;                 % Magnitude of the electron charge.

% the magnetic field:
    Btot = [Bx By Bz];

% the resulting cross product for the force balance, with prefactor
% e/m from ma = ev x B:

    dvdtlorentz=e/mEff*cross(v,Btot);

% the resulting three differential equation contributions for the ODE
% solver:
    out1 = [dvdtlorentz(1);dvdtlorentz(2);dvdtlorentz(3)];
```

Particleadder.m:

```
% This program will merge together files (of 250 particles) generated by
% parallel runs of the masterprogram. It assumes that the files have been
% renamed, in the form "file_1.m", "file_2.m" etc, and then merges them
% into a file named "file.m". These latter files are then used to generate
% the T2* versus angle arrays by the function "readout.m".

% A copy of this program should be placed in the folder containing the
% simulation data, and be run from there. The files for 1000 particles will
% be generated in this same folder. The #-signs should be properly entered,
% depending on the magnetic field the simulation was run for (the B-fields
% should have 2 decimals).


for n=-45:5:135


    file=sprintf('3D alpha=%d.0 B=[#.## #.## #.##]_1.mat',n);
    load(file);
    spinXAveSum=spinXAve;
    spinYAveSum=spinYAve;
    spinZAveSum=spinZAve;
    XplusAll=Xplus;
    XminusAll=Xminus;
    YplusAll=Yplus;
    YminusAll=Yminus;
    ZplusAll=Zplus;
    ZminusAll=Zminus;

    for m=2:4

     file=sprintf('3D alpha=%d.0 B=[#.## #.## #.##]_%d.mat',n,m);
     load(file);
     spinXAveSum = spinXAveSum+spinXAve;
     spinYAveSum = spinYAveSum+spinYAve;
     spinZAveSum = spinZAveSum+spinZAve;
     XplusAll = [XplusAll Xplus];
     XminusAll = [XminusAll Xminus];
     YplusAll = [YplusAll Yplus];
     YminusAll = [YminusAll Yminus];
     ZplusAll = [ZplusAll Zplus];
     ZminusAll = [ZminusAll Zminus];

    end
```

```
    Xplus = XplusAll;
    Xminus = XminusAll;
    Yplus = YplusAll;
    Yminus = YminusAll;
    Zplus = ZplusAll;
    Zminus = ZminusAll;
    spinXAve = spinXAveSum/4;
    spinYAve = spinYAveSum/4;
    spinZAve = spinZAveSum/4;
    spinRAve = sqrt(spinXAve.*spinXAve...
                  + spinYAve.*spinYAve...
                  + spinZAve.*spinZAve);


    keep spinXAve spinYAve spinZAve spinRAve Xplus...
         Xminus Yplus Yminus Zplus Zminus n
    file=sprintf('3D alpha=%d.0 B=[#.## #.## #.##].mat',n);
    save(file);
    clear

end
```

Readout.m:

```
% This program will, for proper input of magnetic fields, load the T2*
% versus time traces, first in different files for different angles, into
% one array named spinravesBis#, which can then be easily used for fitting
% and data extraction.

% A copy of this program should be placed in the folder with the files
% generated by particleadder.m and run from there, and the #-signs should
% be properly entered (the B-fields should have 2 decimals).


load('3D alpha=-45.0 B=[#.## #.## #.##].mat');
spinravesBis#=spinRAve;
XplusBis#=Xplus;
XminusBis#=Xminus;
YplusBis#=Yplus;
YminusBis#=Yminus;
ZplusBis#=Zplus;
ZminusBis#=Zminus;

for n=-40:5:135

    file=sprintf('3D alpha=%d.0 B=[#.## #.## #.##].mat',n);
    load(file);
    spinravesBis#=[spinravesBis#; spinRAve];
    XplusBis#=[XplusBis#;Xplus];
    XminusBis#=[XminusBis#;Xminus];
    YplusBis#=[YplusBis#;Yplus];
    YminusBis#=[YminusBis#;Yminus];
    ZplusBis#=[ZplusBis#;Zplus];
    ZminusBis#=[ZminusBis#;Zminus];
end
```

T2stars.m:

```
% to fit exponents to all traces and determine their T2*:

function[] = T2stars(spinraves)

x=(1:length(spinraves))';
fit = zeros(37,1);
z = zeros(length(spinraves),37);

for m=1:37
    fit(m)=fitexp(x, spinraves(:,m));
    z(:,m)=spinraves(:,m)-exp(-fit(m)*x);
end



alpha = -45:5:135;

% the next line can plot the deviation from exponential behaviour:
% p=plot(alpha,z);
% the following line plots alpha vs T2*:
p=plot(alpha,1./(1999*fit)); % the 1999 comes from the fact that after 1999
                             % 0.5 ps steps, we have come to 1 ns runtime.
```

fitexp.m:

```
function [estimates, model] = fitexp(xdata, ydata)
% Call fminsearch with a random starting point.
start_point = rand(1);
model = @expfun;
estimates = fminsearch(model, start_point);
% expfun accepts curve parameters as inputs, and outputs sse,
% the sum of squares error for exp(-lambda*xdata)-ydata,
% and the FittedCurve.
    function [sse, FittedCurve] = expfun(params)
        lambda = params;
        FittedCurve = exp(-lambda * xdata);
        ErrorVector = FittedCurve - ydata;
        sse = sum(ErrorVector .^ 2);
    end
end
```

Appendix C

CD with matlab code and EBL designs

CD contains:

I. Matlab code II. EBL designs III. This thesis in digital form IV. Images used in this thesis